Alma Mater Studiorum - Università di Bologna

Scuola di Scienze
Dipartimento di Fisica e Astronomia
Corso di Laurea Magistrale in Fisica

Gravitational Waves from Primordial Black Holes in String Inflation

Relatore:
Prof. Michele Cicoli

Correlatore:
Dott. Francisco G. Pedro

Presentata da:
Nicola Pedron

Anno Accademico 2019-2020

Abstract

We consider a model of inflation, called Fibre Inflation, derived from string theory in the framework of type IIB flux compactification and we study the production of primordial black holes due to the gravitational collapse of the curvature perturbations. They are a good candidate for dark matter and if their mass was in the range $M_{PBH} \in [10^{-17} M_\odot, 10^{-13} M_\odot]$ then their contribution to the total dark matter abundance would be between 10% and 100%. The inflaton potential has enough tuning freedom to allow for a flat plateau at large field values, corresponding to the usual slow roll behaviour, and an inflection point near the minimum that enhances the scalar perturbations. It is the latter feature that greatly increases the density anisotropies from the usual $\delta\rho/\rho \sim 10^{-5}$, typical of the CMB radiation, to $\delta\rho/\rho \sim 10^{-1}$ due to a peak in the primordial power spectrum that allows for the formation of black holes. The latter is computed solving the Mukhanov-Sasaki equation numerically using the Hubble slow roll parameters extracted from the solutions to the Friedmann equations and the inflaton equation of motion. The formation of black holes is followed by the production of a stochastic background of secondary gravitational waves: in this thesis we compute their amplitude and compare it with current observational bounds and the sensitivities of earth- and space-based interferometers. Our result is within reach of experiments like DECIGO and BBO, hence in the future it will be possible to have a comparison between our theoretical results and observations.

Abstract

Consideriamo un modello inflazionario, chiamato Fibre Inflation, derivato dalla teoria delle stringhe nell'ambito della compattificazione del flusso di tipo IIB e studiamo la produzione di buchi neri primordiali dovuta al collasso gravitazionale delle perturbazioni di curvatura. Questi sono buoni candidati per la materia oscura e se la loro massa fosse nel range $M_{PBH} \in [10^{-17}M_{\odot}, 10^{-13}M_{\odot}]$ allora il loro contributo all'abbondanza totale di materia oscura sarebbe tra il 10% e il 100%. Il potenziale dell'inflatone presenta sufficiente libertà di tuning per permettere un plateau piatto ad alti valori del campo scalare, corrispondente all'usuale comportamento slow roll, e un punto di flesso vicino al minimo che intensifica le perturbazioni scalari. È quest'ultima caratteristica che aumenta le anisotropie nella densità dall'usuale $\delta\rho/\rho \sim 10^{-5}$, tipiche della radiazione CMB, a $\delta\rho/\rho \sim 10^{-1}$ a causa di un picco nello spettro primordiale che permette la formazione di buchi neri. Lo spettro è calcolato risolvendo numericamente l'equazione di Mukhanov-Sasaki usando i parametri di slow roll di Hubble ricavati dalla soluzione delle equazioni di Friedmann e le equazioni del moto dell'inflatone. La formazione di buchi neri è seguita dalla produzione di un background stocastico di onde gravitazionali secondarie: in questa tesi calcoliamo la loro ampiezza e la confrontiamo con gli attuali limiti osservativi e le sensibilità degli interferometri sulla Terra e nello spazio. Il nostro risultato è entro la portata di esperimenti come DECIGO e BBO, quindi in futuro sarà possibile avere un confronto tra i nostri risultati teorici e le osservazioni.

Contents

1 Introduction and notation **1**

2 Standard cosmology and related issues **3**
2.1 The evolution of the universe . . . 3
2.1.1 The FRW metric . . . 3
2.1.2 A model for the universe: the perfect fluid . . . 4
2.1.3 Friedmann equations . . . 6
2.2 Problems with this scenario . . . 8
2.2.1 Inflation . . . 10

3 Inflation and PBHs **13**
3.1 Dynamics of inflation . . . 13
3.2 Cosmological perturbations . . . 17
3.2.1 Metric perturbations in Minkowski and FRW spacetime . . . 18
3.2.2 Dynamics and quantization of perturbations . . . 20
3.2.3 Scalar power spectrum . . . 23
3.2.4 Tensor power spectrum . . . 24
3.3 Dark Matter and PBHs . . . 26
3.3.1 PBH formation . . . 28

4 Secondary Gravitational Waves from PBH production **30**
4.1 Secondary gravitational waves . . . 30
4.1.1 Some examples . . . 35
4.2 Current observational bounds . . . 39
4.3 Interferometry sensitivity curves . . . 40

5 GWs from Fibre Inflation **43**
5.1 Fibre Inflation . . . 43
5.1.1 PBH formation in Fibre Inflation . . . 45
5.2 GW production in Fibre Inflation . . . 47
5.2.1 Comparison with current observational bounds . . . 50
5.2.2 Comparison with interferometry sensitivity curves . . . 50

6 Conclusions **52**

A Calculations for the broken power law potential **54**

Bibliography **59**

Chapter 1

Introduction and notation

Cosmology is the branch of physics that describes the evolution of the universe and the large scale structures that cannot be dealt with efficiently using classical Newtonian mechanics, such as black holes and galaxies. Its main objective is to comprehend the birth, the history and the fate of our universe taking into account the data collected from observations. But this is not all, as cosmology addresses other important questions concerning high energy physics: in fact when the universe was at its earliest stages of evolution its content was very dense and the energies involved were very high. That is why it is useful to make a link between cosmology and high energy particle physics: in studying early universe cosmology one could virtually obtain a full description of the first stages of its evolution and thus of the mechanisms that triggered and drove it.

However it is not so simple to create the link between cosmology and particle physics. One has to find a concrete framework in which to apply these ideas: for the former the most appropriate one is General Relativity (GR), while for the latter it is Quantum Field Theory (QFT). It is well known that GR as a field theory is non-renormalizable and so when one tries to quantize it its UV behaviour shows some divergences that cannot be removed via the usual renormalization methods. Therefore the QFT of the Standard Model (SM), which is the $SU(3) \times SU(2) \times U(1)$ symmetric theory describing particle physics, treats gravitational interactions only classically, but we know that for some extreme scenarios like the very first moments of the universe or black holes we should rely on a quantum description of gravity. This is a problem that theories like string theory or loop quantum gravity try to solve, but there are ways of dealing with the gravitational interaction of particles making use of some approximations. One of these is QFT in curved spacetime (QFTCS), which is an extension of ordinary QFT, that assumes a flat Minkowski background, to a curved one in which quantum fields evolve. In this context gravity is still treated classically, but the interaction of quantum fields with the gravitational one leads to some crucial consequences, the most famous one being Hawking radiation. QFTCS is the right framework in which we are able to study the evolution of the early universe and therefore it will be our main tool to understand the origin of Primordial Black Holes (PBHs), since as we shall see they are formed due to the curvature perturbation during inflation. The reason why we study PBHs is that because their nature makes them a good candidate for dark matter: in fact they only interact gravitationally with visible matter, which makes them invisible to telescopes, as dark matter should be from observational evidence. The production of

secondary Gravitational Waves (GWs) following PBH formation is then the link between theory and experiments, so a computation of their amplitude and frequency is necessary to perform that connection: this is the objective of this work.

In this thesis we will study the formation of PBHs considering Fibre Inflation, a model of inflation derived from string theory in the framework of type IIB flux compactification. In this scenario inflation is driven by a scalar field, the inflaton, whose potential shows an almost flat plateau at high field values and an inflection point near the minimum. The coupling between the inflaton and the gravitational field leads to an enhancement of the curvature power spectrum that leads to the formation of PBHs. Then we will study the stochastic gravitational waves background produced by this process and we will compare the result with the current bounds given by past observations and with the sensitivities of the earth- and space-based interferometers, both the currently working ones (such as aLIGO and LISA) and the future ones (such as DECIGO and BBO).

Except where it is explicitly indicated we will work in natural units in which $\hbar = c = 1$ until the point where we will introduce the theory of cosmological perturbations, where we will switch to Planck units in which $\hbar = c = G = 1$; the Minkowski metric will be $\eta_{\mu\nu} = \mathrm{diag}(-, +, +, +)$. For the Fourier transformation and its inverse we use the following convention:

$$\tilde{f}(\mathbf{k}) = \frac{1}{(2\pi)^{3/2}} \int_{\mathbb{R}^3} \mathrm{d}^3x \; f(\mathbf{x}) e^{-i\mathbf{k}\cdot\mathbf{x}},$$

$$f(\mathbf{x}) = \frac{1}{(2\pi)^{3/2}} \int_{\mathbb{R}^3} \mathrm{d}^3k \; \tilde{f}(\mathbf{k}) e^{i\mathbf{k}\cdot\mathbf{x}}.$$

Chapter 2

Standard cosmology and related issues

In this chapter we will review some basic concepts of standard cosmology, enlighten its main issues and propose the most elegant and accepted solution, namely inflation.

2.1 The evolution of the universe

2.1.1 The FRW metric

The standard model of cosmology [1][2] relies on the prime assumption of a homogeneous and isotropic universe which goes under the name of *Cosmological Principle* (CP): this comes from the observational fact that the universe looks exactly the same in all directions on sufficiently large scales. As a crucial example one can consider the observation of the *Cosmic Microwave Background* (*CMB*) radiation, whose temperature is about 2.7 K with fluctuations of at most $\delta T/T \sim 10^{-5}$ that can be observed looking far into the deep past of our universe. Figure (2.1) shows the CMB radiation. Once this assumption is considered one can apply it to a concrete framework, namely the one of GR [3][4] and the Einstein gravity theory, whose main starting point are the *Einstein field equations*:

$$R_{\mu\nu} - \frac{1}{2} g_{\mu\nu} R + \Lambda g_{\mu\nu} = 8\pi G T_{\mu\nu}, \tag{2.1}$$

which are partial differential equations for the metric tensor $g_{\mu\nu}$ characterizing the spacetime manifold. In general it is very difficult to find exact solutions to these equations due to their high degree of non-linearity except for few peculiar cases in which there is some symmetry that can be exploited. However there is another way of dealing with cosmology: one can consider a particular form of the metric tensor and insert it into the Einstein equations to have some dynamics. In particular one can show that the CP, i.e. assumption of homogeneity and isotropy, uniquely determines the metric to be the *Friedmann-Robertson-Walker* (FRW) metric:

$$\mathrm{d}s^2 = g_{\mu\nu}\mathrm{d}x^\mu \mathrm{d}x^\nu = -\mathrm{d}t^2 + a^2(t)\left[\frac{\mathrm{d}r^2}{1-kr^2} + r^2 \mathrm{d}\Omega^2\right], \tag{2.2}$$

where $a(t)$ is the cosmological scale factor while $k = 0, \pm 1$ (even though with a suitable rescaling of the coordinates it can assume any real value). These three values correspond to

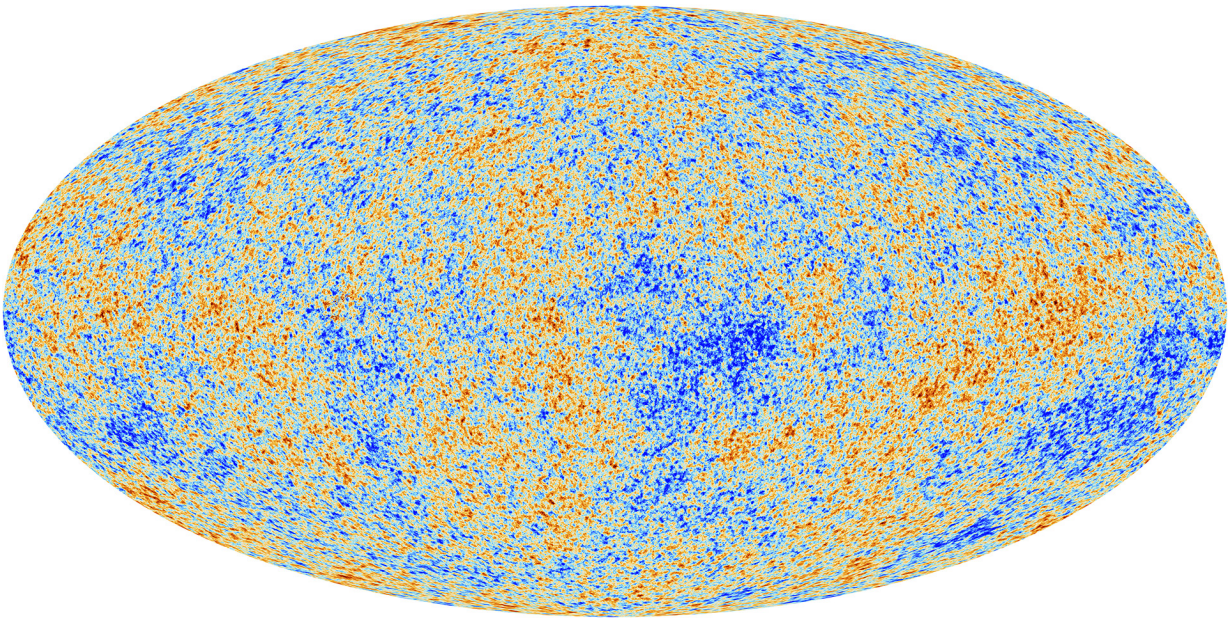

Figure 2.1: The Cosmic Microwave Background as observed by the Planck observatory. The differences in color denote the $\sim 10^{-5}$ energy fluctuations. Source: `https://www.esa.int/ESA_Multimedia/Images/2013/03/Planck_CMB`.

a flat space or a closed/open curved space (de Sitter -dS- or Anti de Sitter -AdS- space). One can also introduce the conformal time τ such that:

$$\mathrm{d}\tau = \frac{\mathrm{d}t}{a(t)},$$

so that we can rewrite the FRW metric as:

$$\mathrm{d}s^2 = a^2(\tau)\left[-\mathrm{d}\tau^2 + \frac{\mathrm{d}r^2}{1-kr^2} + r^2\mathrm{d}\Omega^2\right]. \tag{2.3}$$

Note that for the special case $k = 0$, i.e. flat spacetime, we obtain:

$$\mathrm{d}s^2 = a^2(\tau)\eta_{\mu\nu}\mathrm{d}x^\mu\mathrm{d}x^\nu,$$

where $\eta_{\mu\nu}$ is the Minkowski metric. Hence we can see that for the case of flat spacetime the scale factor $a(\tau)$ acts on distances while it changes in time: the evolution and the expansion of the universe is therefore determined by this parameter, whose dynamics is dictated once we insert the FRW metric into the Einstein equations.

2.1.2 A model for the universe: the perfect fluid

The assumption of homogeneity and isotropy allows us to model the universe as a perfect fluid, for which the stress-energy tensor reads:

$$T_{\mu\nu} = (\rho + p)U_\mu U_\nu - p g_{\mu\nu}, \tag{2.4}$$

where U_μ is the fluid's 4-velocity. For the case of a comoving fluid, for which $U_\mu = (-1, \mathbf{0})$, in a flat FRW background this reduces to $T_{\mu\nu} = \text{diag}(\rho, -p, -p, -p)$. The continuity equation for the stress-energy tensor reads $\nabla_\mu T^\mu_{\ \nu} = 0$ and inserting Eq. (2.4) the $\nu = 0$ component gives:

$$\nabla_\mu T^\mu_{\ 0} = \dot{\rho} + 3H(\rho + p) = 0, \tag{2.5}$$

where the dot $\cdot$ stands for the derivative with respect to the time t while:

$$H = \frac{\dot{a}}{a} \tag{2.6}$$

is the Hubble parameter. One then assumes an equation of state for the fluid, $p = \omega\rho$, then this equation can be rewritten as:

$$\frac{\dot{\rho}}{\rho} = -3(1 + \omega)\frac{\dot{a}}{a}, \tag{2.7}$$

whose general solution is given by:

$$\rho(t) \propto a(t)^{-3(1+\omega)}. \tag{2.8}$$

Let us consider three peculiar values of ω:

- $\omega = 0$: **dust**. In this case the particles composing the fluid don't interact among themselves and so the pressure vanishes. The energy density then reads:

$$\rho_{dust}(t) = \frac{E}{V} \propto a(t)^{-3}. \tag{2.9}$$

  This is compatible with the rescaling of the two quantities determining the energy density. In fact in this limit the fluid can be modeled as cold matter so that the main contribution to the total energy is the mass of the fluid, therefore $\rho_{dust}(t) \approx m/V$. The mass is an invariant quantity so it does not rescale, while the volume rescales as $V \propto a^3$ since any of the three space directions rescales as $x_i \propto a$.

- $\omega = 1/3$: **radiation**. This holds because for massless particles there is no mass scale involved and this implies the trace of the stress-energy tensor to vanish, hence:

$$T = -\rho + 3p = 0 \Longrightarrow p = \frac{1}{3}\rho.$$

  The energy density then reads:

$$\rho_{radiation}(t) \propto a(t)^{-4}. \tag{2.10}$$

  This again is compatible with the rescaling of the two quantities determining the energy density. In fact the photon frequency redshifts as $\nu \propto a^{-1}$ and the volume rescales as $V \propto a^3$.

- $\omega = -1$: **vacuum energy**. In this peculiar case the equation of state becomes:

$$\rho_\Lambda = -p = \frac{\Lambda}{8\pi G}, \tag{2.11}$$

  Λ being the cosmological constant. In such case the energy density does not rescale in time with $a(t)$. We will see later how this is compatible with an accelerated expansion of the universe, i.e. $\ddot{a} > 0$.

In this section we have studied the dependence of the energy density on the scale factor, which by now is an undetermined quantity since Eq. (2.7) is one differential equation for two variables, $\rho(t)$ and $a(t)$. Now we want to examine the dynamics of $a(t)$ and to do it we will work in the frame of GR and Einstein gravity, inserting the FRW metric into the Einstein field equations (2.1).

2.1.3 Friedmann equations

Once we consider the FRW metric and insert it into the Einstein equations we obtain two equations, called the *Friedmann equations*:

$$3\left[\left(\frac{\dot{a}}{a}\right)^2 + \frac{k}{a^2}\right] = 8\pi G\rho, \tag{2.12}$$

$$3\frac{\ddot{a}}{a} = -4\pi G(\rho + 3p). \tag{2.13}$$

Technically speaking the first equation is a constraint on the possible initial conditions for $a(0)$ and $\dot{a}(0)$, while the second one is the real dynamical equation for the scale factor $a(t)$. We can also define the density parameter Ω as:

$$\Omega = \frac{8\pi G}{3H^2}\rho =: \frac{\rho}{\rho_{critical}},\ \rho_{critical} := \frac{3H^2}{8\pi G}, \tag{2.14}$$

so that we can rewrite the first Friedmann equation (2.12) as:

$$\Omega - 1 = \frac{k}{a^2H^2}. \tag{2.15}$$

We then have three possible cases depending on the value of ρ:

- $\rho < \rho_{critical}$ or equivalently $\Omega < 1$ or equivalently $k = -1$, which is the case of an open universe;
- $\rho = \rho_{critical}$ or equivalently $\Omega = 1$ or equivalently $k = 0$, which is the case of a flat universe;
- $\rho > \rho_{critical}$ or equivalently $\Omega > 1$ or equivalently $k = 1$, which is the case of a closed universe.

One can also show that the topology of the universe does not change in time, in the sense that if the initial conditions are related to a flat, open or closed universe then its evolution will always lead to a flat, open or closed universe respectively.

The dynamics of the scale factor is therefore dependent on the value of k, which represents the type of universe we live in. Observations tell us that we are very close to $\Omega = 1$ [5], so our universe is (almost) flat: this means that $k = 0$ and we can then solve the Friedmann equations for the three values of ω we considered before. We then have:

- $\omega = 0$, dust, $\rho \propto a^{-3} \Longrightarrow \ddot{a} \propto a^{-2} \Longrightarrow a(t) \propto t^{\frac{2}{3}}$;
- $\omega = 1/3$, radiation, $\rho \propto a^{-4} \Longrightarrow \ddot{a} \propto a^{-3} \Longrightarrow a(t) \propto t^{\frac{1}{2}}$;
- $\omega = -1$, dark energy, $\rho = \Lambda/(8\pi G) = \text{const} \Longrightarrow \ddot{a} = H_0^2 a = (\Lambda/3)a \Longrightarrow a(t) \propto e^{H_0 t}$, and the Hubble parameter is a constant.

From the form of the dynamical Friedmann equation we see that for $\omega > -1/3$, i.e. in our cases of dust and radiation, there is always a time $t = 0$ at which the scale factor $a(t = 0)$ vanishes: this is a particular feature of these Friedmann models for the universe. This is the Big Bang singularity and it is considered to be the starting point of the universe from which we can measure time. This is a singularity of the metric and it is unavoidable with any change of coordinates[1]. We can then give a brief history of the various phases of the universe starting from the initial singularity:

- $\sim 10^{-43}$ s (10^{19} GeV): this corresponds to the Planck time, non-perturbative quantum gravity plays the most important role and we need to address the study of the universe at these scales to more fundamental theories.
- $\sim 10^{-37}$ s (10^{15} GeV): at this time the Grand Unification Theory (GUT) phase transition occurs, at which the strong and electro-weak interactions separate. Also this is the epoch related to the baryon asymmetry and, more importantly for our purposes, *inflation*, a period of accelerated expansion of the universe.
- $\sim 10^{-11}$ s (100 GeV): the electro-weak spontaneous symmetry breaking occurs and the electromagnetic force separates from the weak force.
- $\sim 10^{-5}$ s (200 MeV): quarks and gluons confine into heavier hadrons.
- ~ 0.2 s ($1 - 2$ MeV): primordial neutrinos decouple from the other particles and propagate almost undisturbed, the ratio between the number of protons and neutrons freezes out.
- $\sim 200 - 300$ s (0.05 MeV): nuclear reactions become efficient and so protons and neutrons fuse together to create heavier nuclei in the process of the *primordial nucleosynthesis*.

[1]Conversely to the case of, for example, the Schwarzschild singularity at $r = 2MG$, which can be shown to be a singularity in the coordinates changing to the Kruskal-Szekeres coordinates.

- $\sim 10^{11}$ s (1 eV): this time corresponds to the matter-radiation equality, i.e. the time at which the density of matter and radiation coincide.
- $\sim 10^{13}$ s: free electrons and protons combine to form neutral hydrogen and the universe becomes transparent to the background radiation. This is the time at which the CMB was formed.
- $\sim 10^{15} - 10^{16}$ s: large scale structures start to form.

2.2 Problems with this scenario

As promising as it might seem to be, the picture we just depicted has many problems that cannot be solved if we only considered the Big Bang theory. Three of them are commonly known as the *flatness problem*, the *horizon problem* and the *magnetic monopole problem*. There is a common solution to these issues: a period of accelerated expansion of the universe called *inflation*. Hereafter we briefly discuss these problems and show how inflation solves them at the same time.

The flatness problem The Friedmann equations tell us that once the universe starts with a certain topology, i.e. closed, flat or open depending on the value of the initial energy density which consequently determines k, it will evolve maintaining that topology. In particular we can study the three cases separately:

- $k = -1$, open universe: the first Friedmann equation reads $\Omega - 1 = -(aH)^{-2}$. It is possible to show that in this case the cosmological expansion wins against the gravitational attraction and the universe keeps expanding forever and $\Omega \to 0$ in time.
- $k = +1$, closed universe: the first Friedmann equation reads $\Omega - 1 = (aH)^{-2}$. In this case it is possible to show that the universe is so dense that a gravitational collapse occurs at a certain time $t_{BC} > 0$ and it goes under the name of Big Crunch.
- $k = 0$, flat spacetime: the first Friedmann equation reduces to $\Omega = 1$ at all times. The energy density parameter never changes and the universe maintains its flatness. However this fixed point is an unstable fixed point since the smallest fluctuation from this value will result in a non-zero curvature that, as we just saw, will result in an indefinitely expanding universe or in a Big Crunch.

As we mentioned before, observations suggest that nowadays our universe is very close to $k = 0$ or equivalently $\Omega_0 = 1$ (the current bound is $|\Omega_0 - 1| = 0.000 \pm 0.005$). Now we are in a dark energy (or vacuum energy) dominated era, so the energy density is constant and equal to the energy density at the moment of the matter-dark energy equality. Using the Friedmann equations it can be shown that we can write the evolution of Ω during the matter domination era as:

$$\Omega(t) - 1 = \frac{(\Omega_0 - 1)a(t)^2}{\Omega_{rad,0} + a(t)\Omega_{matter,0}}, \; a \ll a_{m\Lambda},$$

where $a_{m\Lambda}$ stands for the scale factor at matter-dark energy equality. Considering the time at the matter-radiation equality, at which $a_{rm} \sim 10^{-4}$, we obtain:

$$|\Omega(t_{rm}) - 1| \sim 10^{-6}.$$

At this point going back in time we can consider a radiation-dominated universe, so using the Friedmann equations we can compute the energy density at the Planck time. In this way we obtain:

$$|\Omega(t_P) - 1| \sim 10^{-62}.$$

We can then state the flatness problem as follows. In order to match the observational result of $|\Omega_0 - 1| = 0.000 \pm 0.005$ the initial conditions of the universe have to satisfy the aforementioned bound for the energy density at Planck time. Also note that going back in time it might be possible that we could have an even more stringent condition since the volume of the universe in this scenario becomes smaller and smaller. The problem is that in principle Ω can take any value from 0 to ∞, so the initial conditions of the universe have to be extremely fine-tuned, and this is not very appealing.

The horizon problem The second issue that the Hot Big Bang model presents is the so-called horizon problem. The latest signals that we can detect from the early universe are the ones from the CMB, a background radiation that fills all of the sky that was formed about 350000 years after the Big Bang and whose temperature is $T \approx 2.73$ K everywhere we look up to one part per 100000. Let us consider a flat universe with $k = 0$, so that the metric reads:

$$\mathrm{d}s^2 = a(\tau)^2 \left[-\mathrm{d}\tau^2 + \mathrm{d}r^2 + r^2 \mathrm{d}\Omega^2\right],$$

then if we consider a null geodesic, i.e. the motion of a photon, the maximal distance that a photon can travel in a time $\Delta t = t_f - t_i$ is given by:

$$\Delta\tau = \int_{t_i}^{t_f} \frac{\mathrm{d}\tilde{t}}{a(\tilde{t})}.$$

In particular we can define the *comoving particle horizon* if $t_i = 0$, i.e.:

$$d_p(t) = \int_0^{t_f} \frac{\mathrm{d}\tilde{t}}{a(\tilde{t})}. \tag{2.16}$$

Now, if the CMB is so homogeneous everywhere we look it means that it must have thermalized and so the photons that were scattering before recombination must have been in causal contact with themselves. According to the Hot Big Bang model this must have happened not too far in the past since (at least almost) all of the particles must have been in causal contact with each other in order to be able to thermalize. Keeping this in mind we can compute the maximum angle in the sky that connects two points that could have been in causal contact during recombination. In general the angle between two equal-time points P, Q can be expressed as $\theta = \Delta r / \Delta R$, where Δr is the proper distance between the two points and ΔR is the proper distance from those points to the earth. Therefore if we considered a photon starting from P at the Big Bang time and arriving to Q at

recombination time (this path corresponds to the maximum distance traveled by a photon before recombination) we have:

$$\theta_{max} = \frac{\tau_{rec} - \tau_{BB}}{\tau_0 - \tau_{rec}} =: \frac{\Delta r_{photon}}{\Delta r_0}.$$

In general we have:

$$\tau_2 - \tau_1 = \int_{t_1}^{t_2} \frac{\mathrm{d}\tilde{t}}{a(\tilde{t})} = \int_{a_1}^{a_2} \frac{\mathrm{d}a}{a^2 H(a)}.$$

One can then use the Friedmann equation to write the Hubble parameter as a function of the scale factor. Inserting the known value for a at the time of recombination the final result yields $\theta_{max} \approx 0.02$. This means that the maximal angle that could connect two photons of the CMB travelling towards each other is $2\theta_{max} \approx 0.04$. Therefore since the whole last scattering surface covers a solid angle of 4π then we can estimate $4\pi/(0.04)^2 \sim 10^4$ causally disconnected patches of sky.

We can then state the flatness problem as follows. How can it be that so many causally disconnected regions of the universe are now at the same exact temperature $T \approx 2.73$ K within one part per 100000?

The exotic particles problem As we mentioned before in the very early universe the electro-weak and strong interactions were merged in a single interaction described by a GUT in which the gauge symmetry group was larger than $G_{SM} = SU(3) \times SU(2) \times U(1)$ (like for example $SU(5)$ or $SO(10)$, of which G_{SM} is a subgroup): this means that there was one single coupling constant but more force carriers than the ones that we know nowadays. Then when the GUT phase transition occurred this force split into the strong and electro-weak interactions. During the early times in which the symmetry was not broken the theory predicts the production of some exotic particles such as magnetic monopoles, massless neutrinos or axions. Concentrating on the case of the magnetic monopole, the theory predicts its mass to be very high, $\sim 10^{16}$ GeV, but they are predicted to be stable. Also according to this theory their numerical density should be of the same order of the one for baryons.

We can then state the exotic particles problem as follows. The GUT is elegant and seems a reasonable continuation of the history of the universe going back in time, but why haven't we detected any of these exotic particles? Another big problem concerning magnetic monopoles is that due to their heavy mass they would give a huge contribution to the energy density that would cause the almost instant gravitational collapse of the universe. So how didn't this ever happen at least until now?

2.2.1 Inflation

There is one common solution to all of the aforementioned problems: a period of accelerated expansion of the universe, called *inflation*, right after the GUT transition. The dynamical cause of this process can be achieved in many ways: in the following chapters we will examine models in which inflation is driven by a single scalar field, called the *inflaton*.

Let us now examine why inflation can solve the three problems we described above. First of all we shall assume that the scale factor changes in time as follows:

$$a(t) \propto \begin{cases} \left(\frac{t}{t_i}\right)^{\frac{1}{2}}, & \text{for } 0 < t < t_i, \text{ radiation domination} \\ \exp[H_0(t-t_i)], & \text{for } t_i < t < t_f, \text{ inflation} \end{cases}$$

Flatness problem Let us rewrite the first Friedmann equation for a universe with non-zero curvature as:

$$|\Omega(t) - 1| = \frac{k}{(aH)^2},$$

and suppose that we have an inflationary phase such that the Hubble parameter is actually a constant while the scale factor grows exponentially. Then we can write:

$$|\Omega(t) - 1| = \frac{k}{H_0^2} e^{-2H_0 t}.$$

Therefore if we compare two different times $t_i,\ t_f$ at the start and at the beginning of inflation we have:

$$\frac{|\Omega(t_f) - 1|}{|\Omega(t_i) - 1|} = e^{-2H_0(t_f - t_i)} =: e^{-2N},$$

where we have defined the *number of efoldings* N as $\mathrm{d}N := \mathrm{d}\log a$. Suppose that for $t \approx t_i$ the curvature was very strong, i.e. $|\Omega(t_i) - 1| \approx 1$ (analog reasoning can be done considering a strong positive curvature), then $|\Omega(t_f) - 1| \approx e^{-2N}$. Recalling the relation between the nowadays value of Ω_0 and its value at any time we can write, reminding that $|\Omega_0 - 1| \leq 0.005$:

$$|\Omega(t_f) - 1| \approx e^{-2N} \leq \frac{0.005\ a_f^2}{\Omega_{r,0} + a_f \Omega_{m,0}}.$$

Comparing this expression with the current values of the energy densities for radiation and matter we arrive at the conclusion that $N \geq 60$. This implies that a sufficiently long period of accelerated expansion can solve the flatness problem.

Horizon problem We stated before that the photons composing the CMB must have been in causal contact in order to thermalize. If we assumed a period of accelerated expansion of the universe these particles could have separated quickly, but they could have had the time to reach thermal equilibrium before this process. Recall that the comoving particle horizon differs from the proper particle horizon, which is given by $D_p(t) = a(t)d_p(t)$. Therefore if we considered for instance an accelerated expansion of the form $a(t) \propto e^{H_0(t-t_i)}$ the proper distance between two points in the sky could have increased so quickly that now they could be causally disconnected even though they were not in the early universe. This explains why we see so many causally disconnected patches at the same exact temperature within one part per 100000.

Exotic particles problem The solution to this problem can be achieved once we assume that inflation started after the GUT phase transition. In fact in this way other magnetic monopoles cannot be produced anymore and the ones that were produced before inflation get smeared out at a very fast rate so that their numerical density becomes exponentially small. This explains why we have never detected a single magnetic monopole.

Until now we only explained what inflation is, but we did not describe any mechanism that could allow for such an event to occur. We will see in the next chapter how this can be achieved in a rather simple way considering a model involving a single scalar field. There are theories that involve more than one scalar field, but we will not consider them since the model that we will take into consideration in the study of GW production is a single field model.

Chapter 3

Inflation and PBHs

In this chapter we will study the basic concepts of inflation, enlightening its causes and conditions. After that we will move to the theory of cosmological perturbations and their quantization, showing how they are related to the formation of Primordial Black Holes.

3.1 Dynamics of inflation

The main framework that is used to study fundamental physics is quantum field theory [6][7]: we will rely on its generalization to quantum field theory in curved spacetime [8][9] since we are dealing with a non-fixed background. We will then study models of inflation [10][11] in which the accelerated expansion of the universe is driven by a scalar field Φ called the *inflaton* which is minimally coupled to the gravitational field. The action of such field in a generic spacetime reads:

$$S[\Phi] = \int \mathrm{d}^4x\sqrt{-g}\mathcal{L}[\Phi] = \int \mathrm{d}^4x\sqrt{-g}\left(-\frac{1}{2}g_{\mu\nu}\partial^\mu\Phi\partial^\nu\Phi - V[\Phi]\right), \tag{3.1}$$

where $g_{\mu\nu}$ is the spacetime metric, g is its determinant and $V[\Phi]$ is the inflaton potential. The dynamics of the inflaton field is determined by the Euler-Lagrange equations:

$$\partial_\mu\frac{\delta(\sqrt{-g}\mathcal{L}[\Phi])}{\delta\partial_\mu\Phi} - \frac{\delta(\sqrt{-g}\mathcal{L}[\Phi])}{\delta\Phi} = 0.$$

Inserting the form of the FRW metric Eq. (2.2) the equation of motion reads:

$$\ddot{\Phi} - \frac{1}{a^2}\nabla^2\Phi + 3H\dot{\Phi} + \frac{\delta V[\Phi]}{\delta\Phi} = 0, \tag{3.2}$$

which resembles the Klein-Gordon equation $g_{\mu\nu}\partial^\mu\partial^\nu\Phi + \frac{\delta V[\Phi]}{\delta\Phi} = 0$ weren't it for the a^{-2} factor multiplying the laplacian operator $\nabla^2 = \partial_j\partial^j$ and the friction term $3H\dot{\Phi}$, both coming from the minimal coupling of the inflaton with the gravitational field. We can simplify the discussion adopting a perturbative approach, in which we write the inflaton field as a time-dependent background plus a small perturbation:

$$\Phi(\mathbf{x}, t) = \phi(t) + \delta\phi(\mathbf{x}, t),$$

and study the background first. Its equation of motion reads:

$$\ddot{\phi} + 3H\dot{\phi} + \frac{\delta V[\phi]}{\delta \phi} = 0. \tag{3.3}$$

One can then compute the stress-energy tensor in the usual way as:

$$T_{\mu\nu} = \partial_\mu \phi \partial_\nu \phi + g_{\mu\nu}\mathcal{L},$$

and since ϕ does not depend on space then it is homogeneous and isotropic by construction, so $T_{\mu\nu}$ takes the usual form corresponding to a perfect fluid, $T_{\mu\nu} = \text{diag}(\rho, -p, -p, -p)$. Hence it is possible to obtain the energy density and the pressure:

$$\rho = T_{00} = \frac{\dot{\phi}^2}{2} + V[\phi],\ p = \frac{T^j_{\ j}}{3} = \frac{\dot{\phi}^2}{2} - V[\phi], \tag{3.4}$$

so that we can extract the equation of state parameter ω as:

$$\omega_{infl} = \frac{p}{\rho} = \frac{\frac{\dot{\phi}^2}{2} - V[\phi]}{\frac{\dot{\phi}^2}{2} + V[\phi]}$$

Note that if the kinetic term is subdominant with respect to the potential, i.e. $\dot{\phi}^2 \ll V[\phi]$, then we can obtain an equation of state of the kind $p \approx -\rho$: this condition for the inflaton field is called the *slow roll* condition. As we saw in the previous chapter this corresponds to an exponentially growing scale factor: this means that this scalar field can drive inflation if its potential energy is much larger than its kinetic term (in the following we will see how this translates to some conditions to the inflaton potential).

Let us now consider the first Friedmann equation (2.12), which can be written in an alternative form as:

$$\dot{a}^2 + k = \frac{8\pi G}{3}\rho a^2,$$

then using the form of the energy density ρ given by the inflaton field and considering $k = 0$ we obtain, reminding the definition of the Hubble parameter (2.6):

$$H^2 = \frac{8\pi G}{3}\left(\frac{\dot{\phi}^2}{2} + V[\phi]\right).$$

In order to have inflation the potential must dominate over the kinetic term, hence during inflation we can approximate:

$$H^2 \approx \frac{8\pi G}{3} V[\phi].$$

Since we are considering a model of slow roll inflation then the acceleration $\ddot{\phi}$ can be neglected so that the equation of motion becomes:

$$3H\dot{\phi} + \frac{\delta V[\phi]}{\delta \phi} = 0 \iff \dot{\phi} = -\frac{1}{3H}\frac{\delta V[\phi]}{\delta \phi}$$

The slow roll conditions then become:

$$\dot{\phi}^2 \ll V[\phi] \Longleftrightarrow \frac{1}{V[\phi]}\left(\frac{\delta V[\phi]}{\delta \phi}\right)^2 \ll H^2, \tag{3.5}$$

$$|\ddot{\phi}| \ll |3H\dot{\phi}| \Longleftrightarrow \left|\frac{\delta^2 V[\phi]}{\delta \phi^2}\right| \ll H^2. \tag{3.6}$$

These conditions suggest that the inflaton potential has to be sufficiently flat in order for the field to slowly roll down on it until it reaches the minimum, at which point inflation ends since the potential does not dominate anymore.

Another important consequence of inflation is the shrinking of the comoving Hubble sphere, defined as $r_H := (aH)^{-1}$. In particular one has:

$$\frac{\mathrm{d}}{\mathrm{d}t} r_H = -\left(\frac{\dot{H}}{H^2} + 1\right) = -\frac{\ddot{a}}{\dot{a}^2} < 0,$$

because during inflation $\ddot{a} > 0$. We can then introduce the *Hubble slow roll parameters* ϵ, η and κ, three important quantities that can be used to rewrite the slow roll conditions:

$$\epsilon := -\frac{\dot{H}}{H^2},\ \eta := \frac{\dot{\epsilon}}{\epsilon H},\ \kappa := \frac{\dot{\eta}}{\eta H}.$$

Then the condition for the shrinking of the Hubble sphere can be written as:

$$\frac{\mathrm{d}}{\mathrm{d}t} r_H = \frac{\epsilon - 1}{a} < 0,$$

which tells us that inflation persists as long as $\epsilon < 1$. This also means that the Hubble parameter H changes slowly during inflation. Also as we saw before the inflationary epoch must last for at least $N \geq 60$ so that we can to solve the flatness problem. This implies that the parameter ϵ has to vary slowly, so it must also hold $|\eta| \ll 1$.

Considering the second Friedman equation (2.13), in the same way as we did for the first one we can write it as:

$$\dot{H} + H^2 = -\frac{8\pi G}{3}\left(\frac{\dot{\phi}^2}{2} - V[\phi]\right),$$

and inserting it into the first Friedmann equation we obtain:

$$\dot{H} = -4\pi G \dot{\phi}^2 = -\frac{1}{2M_P^2}\dot{\phi}^2,$$

where we have introduced the reduced Planck mass $M_P = (8\pi G)^{-1/2}$. Therefore we can rewrite the first slow roll parameter as:

$$\epsilon = \frac{1}{2M_P^2}\frac{\dot{\phi}^2}{H^2}. \tag{3.7}$$

Then we can use the slow roll condition $H^2 \approx V[\phi]/(3M_P^2)$ and the equation of motion $\dot{\phi} \approx -\frac{\delta V[\phi]}{\delta \phi}/(3H)$, to write it in terms of the scalar potential as:

$$\epsilon \approx \frac{M_P^2}{2}\left(\frac{1}{V[\phi]}\frac{\delta V[\phi]}{\delta \phi}\right)^2.$$

Analogously we can rewrite η as:

$$\eta \approx M_P^2 \frac{1}{V[\phi]}\frac{\delta^2 V[\phi]}{\delta \phi^2}.$$

Using the above relations we can also write the number of efoldings as a function of the field, in particular:

$$N(\phi) = \int_{t_0}^{t_f} H \mathrm{d}t = \int_{\phi_0}^{\phi_f} \frac{H(\phi)}{\dot{\phi}} \mathrm{d}\phi \approx \int_{\phi_0}^{\phi_f} \frac{1}{M_P\sqrt{2\epsilon(\phi)}} |\mathrm{d}\phi|.$$

Example: $m^2\phi^2$ inflation Let us consider the case of the simplest non-trivial scalar potential:

$$V[\phi] = \frac{1}{2}m^2\phi^2,$$

then the slow roll parameters read:

$$\epsilon = \eta = 2\left(\frac{M_P}{\phi}\right)^2.$$

Since we want these parameters to be small then the inflaton field has to take super-Planckian values until the end, i.e. $\phi > \sqrt{2}M_P =: \phi_f$, then inflation ends. Then we can compute the number of efoldings as:

$$N(\phi) = \int_{\phi_f}^{\phi_0} \frac{\phi}{2M_P^2} \mathrm{d}\phi = \frac{\phi_0^2}{4M_P^2} - \frac{1}{2}.$$

In order to have $N > 60$ it must then hold $\phi_0 > 2\sqrt{60}M_P \approx 15M_P$.

This is an example of a large-field inflation since ϕ takes values which are greater than the Planck mass. There are other models, such as inflection point or hill-top inflation, for which the inflaton field takes values which are sub-Planckian, i.e. $\phi < M_P$.

The inflaton field comes out in other alternative theories to Einstein gravity as well. In particular we know that the Einstein field equations (2.1) are derived from the Einstein-Hilbert action:

$$S_{EH}[g] = \frac{1}{2\kappa^2}\int \mathrm{d}^4x \mathcal{L}_{EH}[g],\ \mathcal{L}_{EH}[g] = \sqrt{-g}R[g],$$

where R is the Ricci scalar and $\kappa = \sqrt{8\pi G}$ is the coupling constant of the theory. As we have seen in this framework the inflaton field is inserted manually in the lagrangian and it is minimally coupled to gravity. There are other theories in which to the Einstein-Hilbert

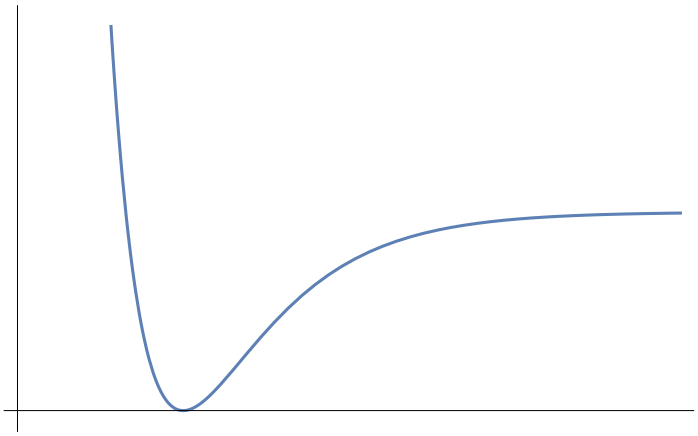

Figure 3.1: A typical inflaton potential. It presents a flat plateau for large field values and a minimum just before an exponentially growing part. The field starts at high values and it slowly rolls down until it reaches the minimum, at which point inflation ends.

action some other terms are added, such as $R^{\mu\nu}R_{\mu\nu}$, $R^{\mu\nu\rho\sigma}R_{\mu\nu\rho\sigma}$ or $f(R)$ [12][13]. In these cases the inflaton field comes out when gauge freedom is exploited to cancel out some degrees of freedom of the gravitational field and its potential looks like the one in figure (3.1). It has an almost flat plateau from which the field rolls down; inflation occurs just before it reaches the minimum, in which it stabilizes and the universe keeps on expanding as usual. In chapter 4 we will not consider the aforementioned cases, but we will see that the inflaton field is one of the moduli that come from string compactification. Its potential can be tuned in order to look like the one in figure (3.1) and in order for it to satisfy the conditions (3.5) and (3.6).

3.2 Cosmological perturbations

In order to derive some observable quantities which will be crucial to compare theoretical predictions with observations we need a framework in which we can define them: this is given by the theory of cosmological perturbations [1][11][14], which we will present here. We will consider this framework because we know that the CMB anisotropies are very small, as we mentioned before. Hence it will be useful to develop the necessary tools to deal with small perturbations of the metric. From now on we will work in Planck units where $\hbar = c = G = 1$.

Suppose we want to study small oscillations of a generic quantity $X(t, \mathbf{x})$ around a value $\bar{X}(t)$, then it is natural to write:

$$X(t, \mathbf{x}) = \bar{X}(t) + \delta X(t, \mathbf{x}),$$

where $\delta X(t, \mathbf{x}) \ll \bar{X}(t)$, $\bar{X}(t)$ being a time-dependent homogeneous and isotropic background. For example we can consider small fluctuations of the metric and the stress-energy tensor:

$$g_{\mu\nu} = \bar{g}_{\mu\nu} + \delta g_{\mu\nu}, \;\; T_{\mu\nu} = \bar{T}_{\mu\nu} + \delta T_{\mu\nu},$$

and in this form we can approximate the Einstein equations to very high accuracy as:

$$\bar{G}_{\mu\nu} = 8\pi\bar{T}_{\mu\nu},\ \delta G_{\mu\nu} = 8\pi\delta T_{\mu\nu},$$

where $G_{\mu\nu}$ is the Einstein tensor and $\delta G_{\mu\nu}$ is its variation given by the variation of the metric and keeping only order $\mathcal{O}(\delta g)$ terms. Also the continuity equation for the stress-energy tensor implies $\nabla_\mu \delta T^\mu_{\ \nu} = 0$.

3.2.1 Metric perturbations in Minkowski and FRW spacetime

If the metric is of the Minkowski type, i.e. $g_{\mu\nu} = \eta_{\mu\nu}$, then the universe is maximally symmetric and we can decompose the metric perturbations into scalar, vector and tensor components (SVT decomposition) which are independent in the linear theory. The perturbed metric can be written as:

$$g_{\mu\nu} = \eta_{\mu\nu} + h_{\mu\nu},$$

where we have denoted $h_{\mu\nu} = \delta g_{\mu\nu}$. We can then categorize the perturbations according to their transformation properties under space rotations. According to this h_{00} is a scalar, h_{0i} are spatial vectors while h_{ij} are spatial tensors. Hence we can parametrize the perturbations in terms of the SVT decomposition as:

$$h_{00} = 2\phi,\ h_{0i} = \beta_i + \partial_i\gamma,\ h_{ij} = -2\psi\delta_{ij} + \left(\partial_i\partial_j - \frac{1}{3}\delta_{ij}\nabla^2\right)\lambda + \frac{1}{2}(\partial_i\epsilon_j + \partial_j\epsilon_i) + h^{TT}_{ij},$$

where $\phi,\ \gamma,\ \psi$ and λ are scalars, β_i and ϵ_i are vectors and h^{TT}_{ij} is a symmetric tensor. We also have the following definition for the laplacian operator and the constraints on the perturbing fields:

$$\nabla^2 = \delta^{ij}\partial_i\partial_j,\ \partial_i\beta^i = 0,\ \partial_i\epsilon^i = 0,\ \partial^i h^{TT}_{ij} = 0,\ \delta^{ij}h^{TT}_{ij} = 0.$$

The "TT" for the tensorial degrees of freedom stands for "transverse-traceless". These conditions imply that the vectors have $3 - 1 = 2$ independent degrees of freedom each while the tensor has $6 - 3 - 1 = 2$ independent degrees of freedom. These expressions can be inverted to give the fields in terms of the metric components if the fields satisfy the following boundary conditions:

$$\gamma \to 0,\ \lambda \to 0,\ \nabla^2\lambda \to 0,\ \epsilon_i \to 0,$$

sufficiently fast at spatial infinity.

The linearized theory is invariant under the gauge transformation $h_{\mu\nu} \to h_{\mu\nu} - \partial_\mu\xi_\nu - \partial_\nu\xi_\mu$. If we write the functions ξ_μ as $\xi_0 = A,\ \xi_i = B_i + \partial_i C$ with $\partial_i B^i = 0$ then the gauge transformations translate as:

$$\delta\phi = -\dot{A},\ \delta\psi = \frac{1}{3}\nabla^2 C,\ \delta\gamma = -A - \dot{C},\ \delta\lambda = -2C,\ \delta\beta_i = -\dot{B}_i,\ \delta\epsilon_i = -2B_i,\ \delta h^{TT}_{ij} = 0,$$

where $\delta X = \tilde{X} - X$ with $\tilde{X}$ being the transformed field. We then see that these fields, except the tensor, are not gauge-invariant. However it is possible to define some gauge-invariant

quantities combining the fields in the right way according to their transformations. In particular we can define the following gauge invariant fields:

$$\Phi := -\phi + \dot{\gamma} - \frac{1}{2}\ddot{\lambda},\ \Psi := -\psi - \frac{1}{6}\nabla^2\lambda,\ \Xi_i := \beta_i - \frac{1}{2}\dot{\epsilon}_i,$$

so that any equation for Φ, Ψ and Ξ_i will be invariant for any gauge choice. As we said before h_{ij}^{TT} is gauge-invariant and it corresponds to gravitational waves. The total number of gauge-invariant degrees of freedom is then six: two of them are given by the two helicity states of h_{ij}^{TT}, two of them are given by the two helicity states of the transverse vector Ξ_i and the other two are given by the two scalars Φ and Ψ. We can then fix a gauge, the most common one being the Newtonian gauge:

$$\gamma = \lambda = 0,\ \beta_i = 0,$$

so that the metric becomes:

$$\mathrm{d}s^2 = -(1-2\phi)\mathrm{d}t^2 + \left[1 - 2\psi + \frac{1}{2}(\partial_i\epsilon_j + \partial_j\epsilon_i) + h_{ij}^{TT}\right]\mathrm{d}x^i\mathrm{d}x^j.$$

Also in this gauge we can write $\psi = -\Psi$, $\phi = -\Phi$ and if we neglect vector perturbations the metric becomes:

$$\mathrm{d}s^2 = -(1+2\Phi)\mathrm{d}t^2 + \left[(1+2\Psi)\delta_{ij} + h_{ij}^{TT}\right]\mathrm{d}x^i\mathrm{d}x^j.$$

Let us now consider the case of an expanding flat FRW spacetime:

$$\mathrm{d}s^2 = g_{\mu\nu}\mathrm{d}x^\mu\mathrm{d}x^\nu = a(\tau)^2\eta_{\mu\nu}\mathrm{d}x^\mu\mathrm{d}x^\nu,$$

which satisfies the condition $g_{\mu\nu} = g_{\mu\nu}(\tau)$. We will perform a change of notation in order to distinguish it from the flat Minkowski case. We can proceed in an analogous way to study perturbations, so we will write the perturbations on the metric as:

$$\delta g_{00} = 2a^2\phi,\ \delta g_{0i} = a^2(S_i + \partial_i B),$$

$$\delta g_{ij} = a^2\left(2\psi\delta_{ij} + 2\partial_i\partial_j E + \partial_i F_j + \partial_j F_i + \frac{1}{2}h_{ij}\right),$$

where ϕ, B, ψ and E are scalars, S_j and F_j are transverse vectors (i.e. $\partial_j S^j = \partial_j F^j = 0$) and h_{ij} is a transverse and traceless tensor (i.e. $\partial_i h^i{}_j = 0$, $h^j{}_j = 0$). In the following we will neglect the vector perturbations since we will not be interested in them. As before h_{ij} is already gauge-invariant, while for the scalar perturbations we define the following gauge-invariant quantities, which take the name of *Bardeen potentials*:

$$\Phi := -\phi + \frac{1}{a}\frac{\mathrm{d}}{\mathrm{d}\tau}\left[a\left(B - \frac{\mathrm{d}E}{\mathrm{d}\tau}\right)\right],\ \Psi := -\psi - \mathcal{H}\left(B - \frac{\mathrm{d}E}{\mathrm{d}\tau}\right),$$

where $\mathcal{H} := a'/a = \dot{a}$ is the conformal Hubble parameter. For $a = 1$ they take a similar form to the case of Minkowski spacetime. Being these quantities gauge invariant we can fix a gauge choice and set again $B = E = 0$, so that $\Psi = -\psi$ and $\Phi = -\phi$. This is called the *conformal Newtonian gauge* and the metric reads:

$$\mathrm{d}s^2 = -a(\tau)^2(1-2\Phi)\mathrm{d}\tau^2 + a(\tau)^2\left[(1-2\Psi)\delta_{ij} + \frac{1}{2}h_{ij}\right]\mathrm{d}x^i\mathrm{d}x^j. \tag{3.8}$$

3.2.2 Dynamics and quantization of perturbations

Until now we studied perturbations around a background without making any assumptions on their nature. Actually the tensor modes are gravitational waves while the scalar modes are related to the *comoving curvature perturbations*, usually denoted by ζ. This is a gauge-invariant quantity whose action reads, at first order:

$$S[\zeta] = \frac{1}{2}\int \mathrm{d}t\mathrm{d}^3x a^3 \frac{\dot{\phi}^2}{H^2}\left[\dot{\zeta}^2 - \frac{1}{a^2}\partial_i\zeta\partial^i\zeta\right], \tag{3.9}$$

We can simplify this equation changing time dependence to conformal time dependence and introducing a new variable, called the *Mukhanov-Sasaki variable*:

$$u := z\zeta,\ z := \sqrt{2\epsilon}a,$$

where ϵ is the first Hubble slow roll parameter. The action then becomes:

$$S[\zeta[u]] = \frac{1}{2}\int \mathrm{d}\tau\mathrm{d}^3x \left[(u')^2 - \partial_i u\partial^i u + \frac{z''}{z}u^2\right]. \tag{3.10}$$

We see that it is very similar to the Klein-Gordon case, but with conformal time and a time-dependent effective mass given by:

$$m_{eff}^2 = -\frac{z''}{z}.$$

The equation of motion for the variable u then reads:

$$u'' - \nabla^2 u - \frac{z''}{z}u = 0. \tag{3.11}$$

We can then define the Fourier modes:

$$u_{\mathbf{k}}(\tau) := \frac{1}{(2\pi)^{3/2}}\int_{\mathbb{R}^3} \mathrm{d}^3x e^{-i\mathbf{k}\cdot\mathbf{x}}u(\tau,\mathbf{x}),$$

so that the equation of motion Eq. (3.11) becomes:

$$u_{\mathbf{k}}'' + \left(k^2 - \frac{z''}{z}\right)u_{\mathbf{k}} = 0. \tag{3.12}$$

This is the *Mukhanov-Sasaki* equation and it will be the starting point to study PBH production during inflation. It is a linear differential equation so its most general solution is given by:

$$u_{\mathbf{k}}(\tau) = a_{\mathbf{k}}^- v_k(\tau) + a_{-\mathbf{k}}^+ v_k^*(\tau),$$

where v_k and v_k^* are two linearly independent solutions and $a_{\pm\mathbf{k}}^{\mp}$ are integration constants. The normalization is chosen to satisfy:

$$W\left[v_k, v_k^*\right] = v_k' v_k^* - v_k v_k^{*\prime} = -i,$$

where $W[v_k, v_k^*]$ is the Wronskian. Also the integration constants are chosen so that:

$$a_{\mathbf{k}}^- = \frac{W\left[v_k, u_{\mathbf{k}}^*\right]}{W\left[v_k, v_k^*\right]},\ a_{\mathbf{k}}^+ = (a_{\mathbf{k}}^-)^*.$$

We can then write the most general solution to the equation of motion (3.11) in terms of these modes as:

$$u(\tau, \mathbf{x}) = \frac{1}{(2\pi)^{3/2}} \int_{\mathbb{R}^3} \mathrm{d}^3k \left[a_{\mathbf{k}}^- v_k(\tau) + a_{-\mathbf{k}}^+ v_k^*(\tau)\right] e^{i\mathbf{k}\cdot\mathbf{x}} = \\ \frac{1}{(2\pi)^{3/2}} \int_{\mathbb{R}^3} \mathrm{d}^3k a_{\mathbf{k}}^- v_k(\tau) e^{i\mathbf{k}\cdot\mathbf{x}} + \text{c.c.} \tag{3.13}$$

We can proceed with the canonical quantization of the theory. As usual we define the conjugate momentum:

$$\pi := \frac{\partial \mathcal{L}}{\partial u'} = u',$$

and promote u and π to the operator valued tempered distributions $\hat{u}$ and $\hat{\pi}$. We then impose equal time canonical commutation relations:

$$[\hat{u}(\tau, \mathbf{x}), \hat{\pi}(\tau, \mathbf{y})] = i\delta^{(3)}(\mathbf{x} - \mathbf{y}),\ [\hat{u}(\tau, \mathbf{x}), \hat{u}(\tau, \mathbf{y})] = [\hat{\pi}(\tau, \mathbf{x}), \hat{\pi}(\tau, \mathbf{y})] = 0,$$

which translate to the commutation relations for the integration constants, which now become the creation and annihilation operators:

$$\left[\hat{a}_{\mathbf{k}}^+, \hat{a}_{\mathbf{p}}^-\right] = \delta^{(3)}(\mathbf{k} - \mathbf{p}),\ \left[\hat{a}_{\mathbf{k}}^+, \hat{a}_{\mathbf{p}}^+\right] = \left[\hat{a}_{\mathbf{k}}^-, \hat{a}_{\mathbf{p}}^-\right] = 0. \tag{3.14}$$

These operators act on the Fock space $\mathcal{F} = \mathbb{C} \oplus (\bigoplus_{n=1}^{\infty} \mathcal{H}_n)$, where:

$$\mathcal{H}_n = \left\{ |\mathbf{k}_1, ..., \mathbf{k}_n\rangle = \frac{1}{\sqrt{n!}} \hat{a}_{\mathbf{k}_n}^+ ... \hat{a}_{\mathbf{k}_1}^+ |0\rangle \right\}$$

is the n-particle Hilbert space and the vacuum state $|0\rangle$ is defined by:

$$\hat{a}_{\mathbf{k}}^- |0\rangle = 0\ \forall \mathbf{k} \in \mathbb{R}^3.$$

Example: Minkowski spacetime Let us consider the example of a flat Minkowski spacetime in which $a = 0$ so that $z''/z = 0$. The Mukhanov-Sasaki equation then becomes:

$$v_k'' + k^2 v_k = 0,$$

whose solution is given by $v_k(\tau) = \alpha e^{-ik\tau} + \beta e^{ik\tau}$. The normalization condition for the modes implies:

$$|\alpha|^2 - |\beta|^2 = \frac{1}{2k},$$

and we can choose $\alpha = 1/\sqrt{2k}$ and $\beta = 0$ so that the modes in Minkowski spacetime become:

$$v_k(\tau) = \frac{1}{\sqrt{2k}} e^{-ik\tau}.$$

The vacuum state $|0\rangle_M$ is unique and from this we can construct the usual unitary Minkowski QFT.

Example: quasi de Sitter spacetime Let us consider the example of a quasi de Sitter spacetime in which $a(\tau) = -1/(H\tau)$ and ϵ is small and approximately constant (in fact during inflation $|\eta| \ll 1$) so that $z''/z = 2/\tau^2$. The Mukhanov-Sasaki equation then becomes:

$$v_k'' + \left(k^2 - \frac{2}{\tau^2}\right) v_k = 0.$$

As initial conditions we impose the so-called *Bunch-Davies conditions*:

$$\lim_{\tau \to -\infty} v_k(\tau) = \frac{1}{\sqrt{2k}} e^{-ik\tau}, \tag{3.15}$$

which basically state that far in the past the modes behave as if they were in Minkowski spacetime. In such case its analytic solution is given by:

$$v_k(\tau) = \frac{1}{\sqrt{2k}} e^{-ik\tau} \left(1 - \frac{i}{k\tau}\right).$$

We can then consider two limits, i.e. the sub-horizon scales $k \gg aH$ and the super-horizon scales $k \ll aH$. We can rewrite the Mukhanov-Sasaki equation for the Fourier modes of the rescaled curvature perturbations $u_{\mathbf{k}}$ as:

$$u_{\mathbf{k}}'' + k^2 \left[1 - 2\left(\frac{aH}{k}\right)^2\right] u_{\mathbf{k}} = 0.$$

Therefore for sub-horizon scales the equation becomes $u_{\mathbf{k}}'' + k^2 u_{\mathbf{k}} = 0$, whose solution is $u_{\mathbf{k}} \propto e^{ik\tau}$. On the other hand for super-horizon scales the equation becomes $u_{\mathbf{k}}'' - 2u_{\mathbf{k}}/\tau^2 = 0$, whose solutions are $u_{\mathbf{k}} \propto \tau^{-1}$ or $u_{\mathbf{k}} \propto \tau^2$, the former being the one of interest. Considering again the curvature perturbations we find that $\zeta_{\mathbf{k}} = u_{\mathbf{k}}/z \propto$ const. This means that curvature perturbations on super-horizon scales freeze: as a consequence it is possible to ignore the evolution of the perturbations from the moment they exited the horizon until today.

Note that the construction of the vacuum is not generally unique in a generic spacetime. In fact, as we said before, Eq. (3.11) is a linear PDE so we can always construct a new solution as a linear combination of known solution. For example we can define some new modes:

$$\tilde{v}_k(\tau) = \alpha_k v_k(\tau) + \beta_k^* v_k^*(\tau),$$

so that we can write the solution to the equation of motion (3.11) using these modes:

$$\hat{u}(\tau, \mathbf{x}) = \frac{1}{(2\pi)^{3/2}} \int_{\mathbb{R}^3} \mathrm{d}^3 k \left[\hat{b}_{\mathbf{k}}^- \tilde{v}_k(\tau) + \hat{b}_{-\mathbf{k}}^+ \tilde{v}_k^*(\tau)\right] e^{i\mathbf{k}\cdot\mathbf{x}} =$$

$$\frac{1}{(2\pi)^{3/2}} \int_{\mathbb{R}^3} \mathrm{d}^3 k \hat{b}_{\mathbf{k}}^- \tilde{v}_k(\tau) e^{i\mathbf{k}\cdot\mathbf{x}} + \text{h.c.}, \tag{3.16}$$

where $\hat{b}_{\mathbf{k}}^{\pm}$ are the new creation and annihilation operators defined by the new modes and they satisfy the same commutation relations Eq. (3.14) provided that $|\alpha_k|^2 - |\beta_k|^2 = 1$

(which is equivalent to $W\left[v_k, v_k^*\right] = -i$). The transformation that relates the two sets of creation and annihilation operators is called *Bogoliubov transformation* and reads:

$$\begin{cases} \hat{a}_{\mathbf{k}}^- = \alpha_k^* \hat{b}_{\mathbf{k}}^- + \beta_k \hat{b}_{-\mathbf{k}}^+ \\ \hat{a}_{\mathbf{k}}^+ = \alpha_k \hat{b}_{\mathbf{k}}^+ + \beta_k^* \hat{b}_{-\mathbf{k}}^- \end{cases} . \tag{3.17}$$

We then have two sets of creation and annihilation operators related by a non trivial transformation which will define two vacuum states:

$$\hat{a}_{\mathbf{k}}^- \left|0\right\rangle_a = 0,\ \hat{b}_{\mathbf{k}}^- \left|0\right\rangle_b = 0\ \forall \mathbf{k} \in \mathbb{R}^3.$$

These are different vacua (in the sense that they cannot be related through a unitary transformation) because the action of an annihilation operator on the vacuum state corresponding to the other set gives something different from 0, in fact:

$$\hat{a}_{\mathbf{k}}^- \left|0\right\rangle_b = \left(\alpha_k^* \hat{b}_{\mathbf{k}}^- + \beta_k \hat{b}_{-\mathbf{k}}^+\right) \left|0\right\rangle_b = \beta_k \hat{b}_{-\mathbf{k}}^+ \left|0\right\rangle_b \neq 0 \text{ if } \beta_k \neq 0.$$

This can also be seen from the definition of the number operator $\hat{N}_{\mathbf{k}}^{(j)} := \hat{j}_{\mathbf{k}}^+ \hat{j}_{\mathbf{k}}^-$, where $\hat{j}$ stands for either $\hat{a}$ or $\hat{b}$. We can then compute the number of particles with momentum $\mathbf{k}$ on any state $\left|\Omega\right\rangle$, in particular we can compute the expectation value of $\hat{N}_{\mathbf{k}}^{(a)}$ on the b vacuum:

$${}_b\!\left\langle 0\right| \hat{N}_{\mathbf{k}}^{(a)} \left|0\right\rangle_b = {}_b\!\left\langle 0\right| \hat{a}_{\mathbf{k}}^+ \hat{a}_{\mathbf{k}}^- \left|0\right\rangle_b = |\beta_k|^2 \delta^{(3)}(\mathbf{0}),$$

where $\delta^{(3)}(\mathbf{0})$ comes from the fact that we are considering an infinite volume, while if we considered the numerical particle density the result would be finite. The non-uniqueness of the vacuum is a consequence of the redefinition of the modes and it is not present in the usual Minkowski QFT since in that case we require the transformations on fields to be unitary. In our case we need an additional condition for the modes that they must satisfy in order to specify the true vacuum of our theory. This is actually given by the Bunch-Davies condition Eq. (3.15) which defines the Bunch-Davies vacuum.

3.2.3 Scalar power spectrum

An important quantity that will be of crucial importance in the study of primordial GWs is the scalar power spectrum $P_u(k)$, which is an observable and it is defined as:

$$\left\langle 0\right| \hat{u}_{\mathbf{k}} \hat{u}_{\mathbf{p}} \left|0\right\rangle = |v_k|^2 \delta^{(3)}(\mathbf{k} + \mathbf{p}) =: P_u(k) \delta^{(3)}(\mathbf{k} + \mathbf{p}), \tag{3.18}$$

together with its dimensionless version:

$$\mathcal{P}_u(k) := \frac{k^3}{2\pi^2} P_u(k). \tag{3.19}$$

This quantity is directly related to the two-point function, which in turn is related to observable quantities: that is why computing the power spectrum is very important to

obtain a link between the theory and observations. To obtain the power spectrum for the curvature perturbations ζ it will be sufficient to divide by z^2 the expression, obtaining:

$$\mathcal{P}_\zeta(k) = \frac{k^3}{2\pi^2}|\zeta_k|^2 = \frac{k^3}{2\pi^2}\left|\frac{u_k}{z}\right|^2. \tag{3.20}$$

The power spectrum can be computed for the case of quasi de Sitter spacetime for super-horizon scales as:

$$P_\zeta(k \ll aH) = \frac{1}{z^2}P_u(k \ll aH) = \frac{1}{2\epsilon a^2}\frac{1}{2k^3\tau^2} = \frac{H^2}{4\epsilon k^3} \Longrightarrow$$

$$\mathcal{P}_\zeta(k) = \frac{H^2}{8\pi^2\epsilon}. \tag{3.21}$$

In our hypothesis $\epsilon < 1$ and $|\eta| \ll 1$, so this can be regarded as a typical slow roll behaviour. Recalling that on super-horizon scales the curvature perturbations freeze then to a good level of approximation we can write the power spectrum at horizon crossing, i.e. $k = aH$, and it becomes just a function of k:

$$\mathcal{P}_\zeta(k = aH) = \left.\frac{H^2}{8\pi^2\epsilon}\right|_{k=aH}.$$

As we said before this is the case for quasi de Sitter, for which both H and ϵ are time-dependent. This means that $\mathcal{P}_\zeta(k)$ is not actually scale invariant and its deviation from scale invariance is described by the *spectral index* n_s defined as:

$$n_s - 1 := \frac{\mathrm{d}\log\mathcal{P}_\zeta(k)}{\mathrm{d}\log k}. \tag{3.22}$$

Both the dimensionless power spectrum and the spectral index are tied by observational constraints [15], which are the following ones:

$$\mathcal{P}_\zeta(k_{\mathrm{CMB}}) = 2 \cdot 10^{-9},$$

$$n_s = 0.9650 \pm 0.0050, \ \frac{\mathrm{d}n_s}{\mathrm{d}\log k} = -0.009 \pm 0.008,$$

where the spectral index and its derivative are computed at scale $k_* = 0.05$ Mpc^{-1} at 68% confidence level.

3.2.4 Tensor power spectrum

When studying GW production associated to PBHs we need to make a distinction between their nature and their origin. In particular we identify three of them [16]:

- "primordial" GWs, which are the ones produced by quantum fluctuations of the metric perturbations;
- "induced" GWs, which are the ones produced when the scalar perturbations re-enter the horizon undergoing gravitational collapse and forming a PBH;

- GW produced by the merging of PBH binaries.

We are interested in the second case, because in the assumption of gaussianity of the scalar perturbations (assumption that we will rely on) no significant primordial GWs are produced [16].

In a similar way to what we did for the scalar case we can define the power spectrum for the tensor modes. In particular if $h_{ij}(\tau, \mathbf{x})$ are the gauge invariant tensor perturbations we can define their Fourier modes as:

$$h_{ij}(\tau, \mathbf{x}) = \frac{1}{(2\pi)^{3/2}} \int_{\mathbb{R}^3} \mathrm{d}^3k \left[h_{\mathbf{k}}^{(+)}(\tau) \mathrm{e}_{ij}^{(+)}(\mathbf{k}) + h_{\mathbf{k}}^{(\times)}(\tau) \mathrm{e}_{ij}^{(\times)}(\mathbf{k}) \right] e^{i\mathbf{k}\cdot\mathbf{x}}, \tag{3.23}$$

where $\mathrm{e}_{ij}^{(+,\times)}(\mathbf{k})$ are the polarization tensors for the + and the × modes. The insertion of the metric in Eq. (3.8) into the Einstein equations and setting the scalar modes to 0 (here we are interested in the tensor modes only) gives, at second order:

$$h_{ij}'' + 2\mathcal{H} h_{ij}' - \nabla^2 h_{ij} = 0,$$

whose solution is Eq. (3.23). In complete analogy with the scalar case we can define the power spectrum for the tensorial modes as:

$$\langle 0 | \, \hat{h}_{\mathbf{k}}^{(m)}(\tau) \hat{h}_{\mathbf{p}}^{(n)}(\tau) \, | 0 \rangle =: \delta^{(3)}(\mathbf{k} + \mathbf{p}) \delta^{(m)(n)} P_h(k), \tag{3.24}$$

where $(m), (n)$ stands for either (+) or (×). Also its dimensionless version is given by:

$$\mathcal{P}_h(k) = \frac{k^3}{2\pi^2} P_h(k). \tag{3.25}$$

As an example we can consider the evolution in conformal time of the tensor modes in quasi de Sitter spacetime. In such case we have:

$$\mathcal{H} = \frac{a'}{a} = -\frac{1}{\tau} \frac{1}{1-\epsilon}.$$

Also in complete analogy to the scalar case, defining a new variable $v_{ij}^{(\cdot)} := a h_{ij}^{(\cdot)}/2$ (where $(\cdot)$ denotes either (+) or (×) polarization state) we can obtain an action that is the same as the one for scalar perturbations, but with two polarization states and $-a''/a$ instead of $-z''/z$ as the effective square mass. For quasi de Sitter spacetime we have:

$$\frac{a''}{a} \approx \frac{1}{\tau^2}(2 + 3\epsilon),$$

and so the solution of the equation of motion, imposing again the Bunch-Davies initial conditions, is given in terms of Hankel functions[1] as:

$$v_{\mathbf{k}}^{(\cdot)}(\tau) = \frac{\sqrt{-\pi\tau}}{2} H_\nu^{(2)}(-k\tau),$$

[1]The Hankel functions of the first and second kind are defined as $H_\nu^{(1,2)}(z) := J_\nu(z) \pm i Y_\nu(z)$, where J_ν and Y_ν are Bessel functions of the first and second kind.

where the index ν is defined as $a''/a =: (\nu^2 - 1/4)/\tau^2$ and in quasi de Sitter spacetime is equal to $\nu \approx 3/2 + \epsilon$. Then it is possible to show that the dimensionless tensor power spectrum for the super-horizon scales is given by:

$$\mathcal{P}_h(k \ll aH) = \left(\frac{k}{aH}\right)^{3-2\nu} \frac{2H^2}{\pi^2}.$$

Therefore it is possible to extract the spectral index for the tensor modes, which is defined as:

$$n_T - 1 := \frac{\mathrm{d}\log \mathcal{P}_h(k)}{\mathrm{d}\log k},$$

and for quasi de Sitter spacetime it is given by $n_T = -2\epsilon$.

We can define the tensor-to-scalar ration r as:

$$r := \frac{\mathcal{A}_T}{\mathcal{A}_s},\ \mathcal{P}_{h,\zeta}(k) =: \mathcal{A}_{T,s}\left(\frac{k}{k_*}\right)^{n_{T,s}-1}. \tag{3.26}$$

Then this is given by $r = 16\epsilon$ in quasi de Sitter spacetime and it is tied to observational constraints, in particular $r_{0.002} < 0.064$ at scale $k_* = 0.002$ Mpc^{-1} [17]. Therefore since we can obtain the consistency relation $r = -8n_T$ then the tensor spectral index is subjected to the same constraints. Note that this holds for single-field inflation, if observations led us to $r \neq -8n_T$ then it would mean that inflation was not driven by a single field.

3.3 Dark Matter and PBHs

The reason why physicists study PBHs is because in the last years the proposal of them being a good candidate for dark matter (DM) arose. The nature of latter is one of the biggest issues in theoretical physics, but its existence solves at least two problems [18].

Galaxy rotation curves These curves give the angular velocity of the stars in a galaxy around its center. For a distribution typical of galaxies they present a maximum near the center and then the velocity decreases far from it. However observations show that once the velocity reaches its maximum it remains almost flat: this can only happen if the mass within the radius increases linearly. This goes in contrast with the observations, which show a decreasing density of usual baryonic matter, see figure (3.2). A solution to this problem is the inclusion of an invisible massive component of the galaxy that permeates it everywhere. We call this Dark Matter (DM) since it does not interact via EM interactions so it cannot be observed directly with any telescope.

Velocity dispersion In a classical bound N-body system the virial theorem must be obeyed. It relates the kinetic energy of the particles with their interaction potential and it can be used to compare the velocity distribution of stars predicted by the theory given the observed (baryonic) mass distribution with observations. The result is not the one that is computed: even considering complicated mass distributions the observations do not match the theoretical predictions. The solution to this problem is again DM because a bigger

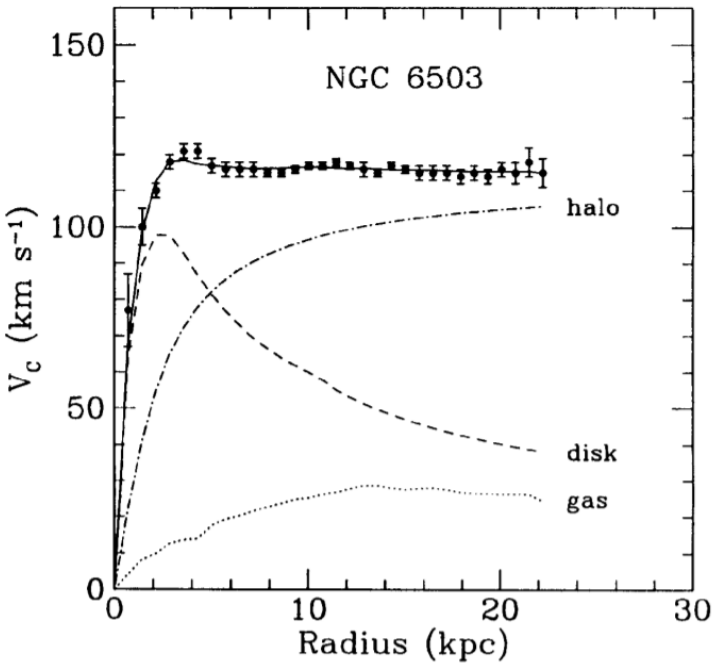

Figure 3.2: The rotation curve for the galaxy NGC 6503 which shows the measured values and the ones given by the theoretical predictions. Source: [18].

mass would match the observations and since it is not detected then it should not interact electro-magnetically.

But what is DM? Its nature is not clear yet and there are many hypothesis, among which we have the following ones:

- Weakly Interacting Massive Particle (WIMP), which should be a new elementary particle not present in the SM and that would be predicted for example by super-symmetric theories (in this case the candidate would be the Lightest Supersymmetric Particle -LSP-) or Kaluza-Klein theories (in this case the candidate would be the Lightest KK Particle -LKP-);
- Quantum Chromodynamics (QCD) axion, which would be a solution to the strong CP problem in the framework of the Peccei-Quinn theory;
- sterile neutrino, which could be a right-handed neutrino inserted in theories beyond the SM to explain neutrino oscillations and it would have a wide mass range, between 1 eV and 10^{15} GeV;
- Gravitationally Interacting Massive Particle (GIMP), which would be arising as massive singularities in the theory of Einstein gravity.

In any case DM should share the same properties: it must be massive, so that it interacts gravitationally, and neutral, so that it does not interact electro-magnetically. We will work

in the different hypothesis that DM is composed of Primordial Black Holes (PBHs), so that we do not have to neither change GR nor add new elementary particles.

3.3.1 PBH formation

Primordial Black Holes [19][20] form when the curvature perturbations re-enter the Hubble horizon during inflation and collapse gravitationally. Their formation was studied in depth by Stephen Hawking in [19]. The main difference between PBHs and "ordinary" black holes is that due to their production mechanism their lower bound on the mass is not $\approx 3\ M_\odot$, which is the minimum mass that a star must have in order to collapse into a black hole. Actually their lower bound is related to gamma ray burst due to Hawking evaporation and it is $M \sim 10^{-17} M_\odot$ [21].

We can write the fraction of the total energy density of PBHs with mass M at formation as [22]:

$$\beta_f(M) = \left.\frac{\rho_{PBH}}{\rho_{tot}}\right|_f,$$

and assuming a gaussian distribution for the curvature perturbations this can be written as:

$$\beta_f(M) = \frac{1}{\sqrt{2\pi}\sigma_M} \int_{\zeta_c}^{\infty} \mathrm{d}\zeta e^{-\frac{\zeta^2}{2\sigma_M^2}},$$

where ζ_c is the critical value for the collapse into a PBH to occur. For $\sigma_M \ll \zeta_c$ we can approximate this expression as:

$$\beta_f(M) \approx \frac{\sigma_M}{\sqrt{2\pi}\zeta_c} e^{-\frac{\zeta_c^2}{2\sigma_M^2}}.$$

The mass of a PBH is assumed to be proportional to the horizon mass M_H, i.e.:

$$M = \gamma M_H = \gamma \left.\frac{4\pi}{3}\frac{\rho_{tot}}{H^3}\right|_f = \frac{4\pi\gamma}{H_f}, \tag{3.27}$$

where γ is a constant related to the details and the efficiency of the gravitational collapse and it is assumed to be $0 \leq \gamma \leq 1$. In our hypothesis PBHs behave as matter, therefore the fraction of the total energy density of PBHs at formation time can be related to the present one as:

$$\beta_f(M) = \left(\frac{H_0}{H_f}\right)^2 \frac{\Omega_{DM}}{a_f^3} f_{PBH}(M),$$

where a_f is the scale factor at formation time, H_0, H_f is the Hubble parameter today and at formation time respectively and Ω_{DM} is the density parameter for DM today which is $\Omega_{DM} \approx 0.26$. Since we assume that the formation of PBHs occurs during the radiation dominated epoch the Hubble parameter behaves as:

$$H_f^2 = \Omega_r \frac{H_0^2}{a_f^4} \left(\frac{g_{*f}}{g_{*0}}\right)^{\frac{1}{3}}, \tag{3.28}$$

where g_{*f} and g_{*0} are the number of relativistic degrees of freedom at PBH formation time and today respectively while Ω_r is the density parameter for radiation which is $\Omega_r \approx 8\times10^{-5}$. Combining these results we can write:

$$\beta_f(M) \approx \frac{4}{\sqrt{\gamma}} \times 10^{-9} \left(\frac{g_{*f}}{g_{*0}}\right)^{\frac{1}{4}} \left(\frac{M}{M_\odot}\right)^{\frac{1}{2}} f_{PBH}(M).$$

Assuming that PBHs constitute all of DM today, i.e. $f_{PBH}(M) = 1\ \forall M$, considering only SM degrees of freedom so that $g_{*f} = 106.75$ and $g_{*0} = 3.36$ and assuming $\gamma = 1$ we obtain:

$$\beta_f(M) \approx 10^{-8} \left(\frac{M}{M_\odot}\right)^{\frac{1}{2}}. \tag{3.29}$$

Since the standard deviation of the gaussian distribution is related to the two-point function as $\sigma_M^2 \sim \langle\zeta\zeta\rangle$ then assuming $\zeta_c = 1$ and $M = 10^{-15}M_\odot$ we find $\beta_f(M) \approx 3 \times 10^{-16}$ and $\sigma = 0.12$. This means that in order to achieve the formation of PBHs we need to enhance the curvature perturbations power spectrum to $\mathcal{O}(10^{-2})$, which is 7 orders of magnitude larger than its value at CMB scales. This enhancement can be achieved in models in which the inflaton potential presents a rich structure that allows for an extremely flat and sufficiently long plateau during the last stages of inflation. This is actually the case for Fibre Inflation, as we will discuss below.

It is also possible to give an estimate of the PBH mass in terms of the number of efoldings that elasped from the CMB scales to their formation. This can be achieved inserting eq. (3.28) into eq. (3.27) and inverting. In particular we have:

$$\Delta N_{\rm CMB}^{\rm PBH} = \log\left(\frac{a_{\rm PBH}H_{\rm inf}}{a_{\rm CMB}H_{\rm inf}}\right) =$$

$$18.4 - \frac{1}{12}\log\left(\frac{g_{*f}}{g_{*0}}\right) + \frac{1}{2}\log\gamma - \frac{1}{2}\log\left(\frac{M}{M_\odot}\right), \tag{3.30}$$

where g_{*f} and g_{*0} are the number of relativistic degrees of freedom at formation time and at current time.

Chapter 4

Secondary Gravitational Waves from PBH production

In this chapter we discuss the theory of secondary gravitational waves induced by a primordial power spectrum and we study some examples. We then present the current observational bounds and the sensitivity curves of interferometers, with which we compare the theoretical results presented in the examples.

4.1 Secondary gravitational waves

To study secondary gravitational waves we will follow [23] (note the different convention for the Fourier transformation in the paper, therefore some definitions will be different). Further details can be found in [24] and [25]. Let us consider the following perturbed metric in the conformal Newtonian gauge:

$$\mathrm{d}s^2 = -a(\tau)^2(1+2\Psi)\mathrm{d}\tau^2 + a(\tau)^2\left[(1-2\Psi)\delta_{ij} + \frac{1}{2}h_{ij}\right]\mathrm{d}x^i\mathrm{d}x^j,$$

where $\Psi,\ \Phi\ (= -\Psi$ in the absence of anisotropic stress) are the Bardeen potentials while $\partial_i h^{ij} = 0,\ h = h^j{}_j = 0$. We can write the tensor perturbations expanding in Fourier modes:

$$h_{ij}(\tau, \mathbf{x}) = \frac{1}{(2\pi)^{3/2}}\int_{\mathbb{R}^3}\mathrm{d}^3k\left[h_{\mathbf{k}}^{(+)}(\tau)\mathrm{e}_{ij}^{(+)}(\mathbf{k}) + h_{\mathbf{k}}^{(\times)}(\tau)\mathrm{e}_{ij}^{(\times)}(\mathbf{k})\right]e^{i\mathbf{k}\cdot\mathbf{x}},$$

where we have defined the polarization tensors:

$$\mathrm{e}_{ij}^{(+)}(\mathbf{k}) = \frac{1}{\sqrt{2}}\left[u_i(\mathbf{k})u_j(\mathbf{k}) - v_i(\mathbf{k})v_j(\mathbf{k})\right],$$

$$\mathrm{e}_{ij}^{(\times)}(\mathbf{k}) = \frac{1}{\sqrt{2}}\left[u_i(\mathbf{k})v_j(\mathbf{k}) + v_i(\mathbf{k})u_j(\mathbf{k})\right],$$

where $\mathbf{u}$ and $\mathbf{v}$, which have both unitary norm, are three-vectors defined in such a way that $(\mathbf{u}, \mathbf{v}, \hat{k} = \mathbf{k}/|\mathbf{k}|)$ form an orthonormal triplet.

We can then insert the perturbed metric in the Einstein equations and expand them up to second order to obtain the evolution equation for the secondary GWs. This reads:

$$h''_{ij} + 2\mathcal{H}h'_{ij} - \nabla^2 h_{ij} = -4\mathcal{P}^{rs}_{ij}\mathcal{S}_{rs},$$

where a prime $'$ denotes a derivation with respect to the conformal time τ, $\mathcal{H} = a'/a = aH$ is the conformal Hubble parameter, $\mathcal{P}^{rs}_{ij}$ is the projection operator to the transverse and traceless part of the source term $\mathcal{S}_{rs}$. We can then move to the conjugate space via Fourier transformation:

$$\hat{\mathcal{S}}_{rs}(\tau, \mathbf{k}) = \frac{1}{(2\pi)^{3/2}} \int_{\mathbb{R}^3} \mathrm{d}^3x \mathcal{S}_{rs}(\tau, \mathbf{x}) e^{-i\mathbf{k}\cdot\mathbf{x}},$$

$$\hat{\mathcal{P}}^{rs}_{ij} = \mathrm{e}^{(+)}_{ij}(\mathbf{k})\mathrm{e}^{(+)rs}(\mathbf{k}) + \mathrm{e}^{(\times)}_{ij}(\mathbf{k})\mathrm{e}^{(\times)rs}(\mathbf{k}),$$

so that the equation of motion becomes:

$$\frac{\mathrm{d}^2}{\mathrm{d}\tau^2} h^{(\cdot)}_{\mathbf{k}}(\tau) + 2\mathcal{H}\frac{\mathrm{d}}{\mathrm{d}\tau} h^{(\cdot)}_{\mathbf{k}}(\tau) + k^2 h^{(\cdot)}_{\mathbf{k}}(\tau) = \hat{\mathcal{S}}^{(\cdot)}(\tau, \mathbf{k}),$$

where $(\cdot)$ denotes either $(+)$ or $(\times)$ and $\hat{\mathcal{S}}^{(\cdot)}(\tau, \mathbf{k}) := -4\mathrm{e}^{(\cdot)rs}(\mathbf{k})\hat{\mathcal{S}}^{(\cdot)}_{rs}(\tau, \mathbf{k})$. The solution to the equation can be expressed in terms of a Green function $g_{\mathbf{k}}$ for a radiation dominated universe ($k = |\mathbf{k}|$):

$$h^{(\cdot)}_{\mathbf{k}}(\tau) = \frac{1}{a(\tau)} \int_{\tau_0}^{\tau} \mathrm{d}\tilde{\tau} g_{\mathbf{k}}(\tau, \tilde{\tau}) a(\tilde{\tau}) \hat{\mathcal{S}}^{(\cdot)}(\tilde{\tau}, \mathbf{k}),$$

$$g_{\mathbf{k}}(\tau, \tilde{\tau}) = \frac{\sin[k(\tau - \tilde{\tau})]}{k} \theta(\tau - \tilde{\tau}). \tag{4.1}$$

From the expansion of the Einstein equations we can then obtain the source term at second order in the scalar. We are considering a radiation dominated era, hence $\omega = 1/3$, therefore we have:

$$\mathcal{S}_{ij} = 4\Psi\partial_i\partial_j\Psi + 2\partial_i\Psi\partial_j\Psi - \frac{4}{3(1+\omega)}\partial_i\left(\frac{\Psi'}{\mathcal{H}} + \Psi\right)\partial_j\left(\frac{\Psi'}{\mathcal{H}} + \Psi\right) =$$

$$4\Psi\partial_i\partial_j\Psi + 2\partial_i\Psi\partial_j\Psi - \partial_i\left(\frac{\Psi'}{\mathcal{H}} + \Psi\right)\partial_j\left(\frac{\Psi'}{\mathcal{H}} + \Psi\right).$$

We need to write it in Fourier space. First we define the usual Fourier modes for the scalar $\hat{\Psi}(\tau, \mathbf{k})$:

$$\hat{\Psi}(\tau, \mathbf{k}) = \frac{1}{(2\pi)^{3/2}} \int_{\mathbb{R}^3} \mathrm{d}^3x \Psi(\tau, \mathbf{x}) e^{-i\mathbf{k}\cdot\mathbf{x}}.$$

They are related to the curvature perturbations ζ through the relation $\Psi = \frac{2}{3}\zeta$ and we can write them in terms of a transfer function:

$$\hat{\Psi}(\tau, \mathbf{k}) = T(\tau, \mathbf{k})\hat{\Psi}(\mathbf{k}) = \frac{2}{3}T(\tau, \mathbf{k})\hat{\zeta}(\mathbf{k}),$$

where:

$$T(\tau, \mathbf{k}) = \mathcal{T}(k\tau), \ \mathcal{T}(x) = \frac{9}{x^2}\left[\frac{\sin\left(x/\sqrt{3}\right)}{x/\sqrt{3}} - \cos\left(x/\sqrt{3}\right)\right]$$

is the expression of the transfer function in the radiation dominated era. We further define the following function:

$$f(\tau, k_1, k_2) = 4\left[2T(\tau, k_1)T(\tau, k_2) + \left(T(\tau, k_1) + \frac{T'(\tau, k_1)}{\mathcal{H}}\right)\left(T(\tau, k_2) + \frac{T'(\tau, k_2)}{\mathcal{H}}\right)\right], \tag{4.2}$$

then the final result for the Fourier transformed of the source term yields:

$$\hat{\mathcal{S}}^{(\cdot)}(\tau, \mathbf{k}) = \frac{1}{(2\pi)^{3/2}}\frac{4}{9}\int_{\mathbb{R}^3} \mathrm{d}^3p\ \mathrm{e}^{(\cdot)}(\mathbf{k}, \mathbf{p}) f(\tau, p, |\mathbf{k}-\mathbf{p}|)\zeta(\mathbf{p})\zeta(\mathbf{k}-\mathbf{p}),$$

where $\mathrm{e}^{(\cdot)}(\mathbf{k}, \mathbf{p}) = \mathrm{e}^{(\cdot)jk}(\mathbf{k})p_j p_k$. This expression for the source term can then be inserted into the solution to the GW equation of motion. In particular we obtain:

$$h^{(\cdot)}_{\mathbf{k}}(\tau) = \frac{1}{(2\pi)^{3/2}}\frac{4}{9}\int_{\mathbb{R}^3} \mathrm{d}^3p \frac{1}{k^3\tau}\mathrm{e}^{(\cdot)}(\mathbf{k}, \mathbf{p})\zeta(\mathbf{p})\zeta(\mathbf{k}-\mathbf{p}) \cdot ...$$

$$... \cdot \left[\int_{\tau_0}^{\tau} k\mathrm{d}\tilde{\tau}(k\tilde{\tau})\left(\sin(k\tau)\cos(k\tilde{\tau}) - \cos(k\tau)\sin(k\tilde{\tau})\right) f(\tilde{\tau}, p, |\mathbf{k}-\mathbf{p}|)\right].$$

Now we need to determine the extremes of the integration over $\tilde{\tau}$. For the lower one we can consider $\tau_0 = 0$ since inflation occurs at the very early stages of the evolution of the universe. In order to fix the upper extreme of integration we need to study the behaviour of the transfer function $T(\tau, k)$ and of the function $f(\tau, k_1, k_2)$. As we said before the tensor modes are generated when the perturbations re-enter the Hubble horizon. Since the transfer function decays as τ^{-2} this process ends at a time which is around $\tau \approx \mathcal{O}(10^3)k^{-1}$: this implies that we can approximate the upper extreme of integration to $\tau \to \infty$. Hence the tensor modes become:

$$h^{(\cdot)}_{\mathbf{k}}(\tau) = \frac{1}{(2\pi)^{3/2}}\frac{4}{9}\int_{\mathbb{R}^3} \mathrm{d}^3p \frac{1}{k^3\tau}\mathrm{e}^{(\cdot)}(\mathbf{k}, \mathbf{p})\zeta(\mathbf{p})\zeta(\mathbf{k}-\mathbf{p}) \cdot ...$$

$$... \cdot \left[\mathcal{I}_c\left(\frac{p}{k}, \frac{|\mathbf{k}-\mathbf{p}|}{k}\right)\cos(k\tau) + \mathcal{I}_s\left(\frac{p}{k}, \frac{|\mathbf{k}-\mathbf{p}|}{k}\right)\sin(k\tau)\right],$$

where we have defined the functions:

$$\mathcal{I}_c(x, y) := \int_0^{\infty} \mathrm{d}z z(-\sin z)\chi(x, y; z)$$

$$\mathcal{I}_s(x, y) := \int_0^{\infty} \mathrm{d}z z(\cos z)\chi(x, y; z)$$

$$\chi(x, y; z) := 4\left[2\mathcal{T}(xz)\mathcal{T}(yz) + \left(\mathcal{T}(xz) + xz\frac{\partial}{\partial z}\mathcal{T}(xz)\right)\left(\mathcal{T}(xz) + xz\frac{\partial}{\partial z}\mathcal{T}(xz)\right)\right].$$

If we define the new coordinates $x := p/k,\ y := |\mathbf{k}-\mathbf{p}|/k$ and we assume that the curvature perturbation only depend on the modulus of the mode k and not on its direction then the

domain of integration for these coordinates allowed by the triangular inequality for the triplet $(\mathbf{k}, \mathbf{p}, \mathbf{k}-\mathbf{p})$ is given by:

$$x+y \geq 1 \ \cap \ x-y \geq -1 \ \cap \ x-y \leq 1.$$

We can then perform another coordinate transformation, $d := |x-y|/\sqrt{3}, \ s := (x+y)/\sqrt{3}$, and the domain of integration simply becomes $0 \leq d \leq 1/\sqrt{3}, \ 1/\sqrt{3} \leq s < \infty$. In doing so the integrals $\mathcal{I}_c$ and $\mathcal{I}_s$ can be computed analytically.

In general observables are related to correlation functions. In our case we want to compute the two-point function of the tensor modes since, as we shall see later, it is related to the energy density parameter of GWs.

The two-point function is given by the insertion of the Fourier modes into a correlator:

$$\langle h^{(m)}_{\mathbf{k}_1}(\tau) h^{(n)}_{\mathbf{k}_2}(\tau)\rangle = \frac{1}{(2\pi)^3}\left(\frac{4}{9}\right)^2 \int_{\mathbb{R}^3} \mathrm{d}^3 p_1 \int_{\mathbb{R}^3} \mathrm{d}^3 p_2 \frac{1}{k_1^3 k_2^3 \tau^2} \mathrm{e}^{(m)}(\mathbf{k}_1, \mathbf{p}_1) \mathrm{e}^{(n)}(\mathbf{k}_2, \mathbf{p}_2) \cdot ...$$

$$... \cdot \langle \zeta(\mathbf{p}_1)\zeta(\mathbf{k}_1-\mathbf{p}_1)\zeta(\mathbf{p}_2)\zeta(\mathbf{k}_2-\mathbf{p}_2)\rangle \cdot ...$$

$$... \cdot \left[\mathcal{I}_c(x_1, y_1)\cos(k_1\tau) + \mathcal{I}_s(x_1, y_1)\sin(k_1\tau)\right]\left[\mathcal{I}_c(x_2, y_2)\cos(k_2\tau) + \mathcal{I}_s(x_2, y_2)\sin(k_2\tau)\right],$$

where we used $(m, n) = (+), (\times)$ to define the two polarization states and $x_j, \ y_j$ are the same coordinates that we defined earlier. We also highlighted the four-point function for the curvature perturbations $\langle \zeta(\mathbf{p}_1)\zeta(\mathbf{k}_1-\mathbf{p}_1)\zeta(\mathbf{p}_2)\zeta(\mathbf{k}_2-\mathbf{p}_2)\rangle$. Recalling the definition of the dimensionless scalar power spectrum $\mathcal{P}_\zeta(k_1)$:

$$\langle \zeta(\mathbf{k}_1)\zeta(\mathbf{k}_2)\rangle = \delta^{(3)}(\mathbf{k}_1+\mathbf{k}_2)\frac{2\pi^2}{k_1^3}\mathcal{P}_\zeta(k_1),$$

we can express the four-point function exploiting Wick theorem and checking the admissible configuration for the momenta. The result is:

$$\langle \zeta(\mathbf{p}_1)\zeta(\mathbf{k}_1-\mathbf{p}_1)\zeta(\mathbf{p}_2)\zeta(\mathbf{k}_2-\mathbf{p}_2)\rangle =$$

$$\delta^{(3)}(\mathbf{k}_1+\mathbf{k}_2)\left[\delta^{(3)}(\mathbf{k}_2+\mathbf{p}_1-\mathbf{p}_2) + \delta^{(3)}(\mathbf{p}_1+\mathbf{p}_2)\right]\frac{2\pi^2}{p_1^3}\frac{2\pi^2}{|\mathbf{k}_1-\mathbf{p}_1|^3}\mathcal{P}_\zeta(k_1)\mathcal{P}_\zeta(|\mathbf{k}_1-\mathbf{p}_1|).$$

hence the two-point function for the tensor modes becomes:

$$\langle h^{(m)}_{\mathbf{k}_1}(\tau) h^{(n)}_{\mathbf{k}_2}(\tau)\rangle = \delta^{(3)}(\mathbf{k}_1+\mathbf{k}_2)\cdot 2\left(\frac{4}{9}\right)^2 \int_{\mathbb{R}^3} \mathrm{d}^3 p_1 \frac{1}{k_1^6\tau^2} \mathrm{e}^{(m)}(\mathbf{k}_1, \mathbf{p}_1)\mathrm{e}^{(n)}(\mathbf{k}_1, \mathbf{p}_1) \cdot ...$$

$$... \cdot \frac{2\pi^2}{p_1^3}\frac{2\pi^2}{|\mathbf{k}_1-\mathbf{p}_1|^3}\mathcal{P}_\zeta(k_1)\mathcal{P}_\zeta(|\mathbf{k}_1-\mathbf{p}_1|) \cdot ...$$

$$... \cdot \left[\cos^2(k_1\tau)\mathcal{I}_c^2(x_1, y_1) + \sin^2(k_1\tau)\mathcal{I}_s^2(x_1, y_1) + \sin(2k_1\tau)\mathcal{I}_c(x_1, y_1)\mathcal{I}_s(x_1, y_1)\right].$$

We can then express the integral in terms of the variables x and y, which turns out to be:

$$\langle h^{(m)}_{\mathbf{k}_1}(\tau) h^{(n)}_{\mathbf{k}_2}(\tau)\rangle = \delta^{(3)}(\mathbf{k}_1+\mathbf{k}_2)\frac{2\pi^2}{k_1^3}\delta^{(m)(n)} \cdot \frac{4}{81}\frac{1}{k_1^2\tau^2} \cdot ...$$

$$... \cdot \iint_{\mathcal{A}} \mathrm{d}x\mathrm{d}y \frac{x^2}{y^2}\left[1-\frac{(1+x^2-y^2)^2}{4x^2}\right]^2 \mathcal{P}_\zeta(k_1 x)\mathcal{P}_\zeta(k_1 y)\cdot ...$$
$$... \cdot \left[\cos^2(k_1\tau)\mathcal{I}_c^2(x_1,y_1)+\sin^2(k_1\tau)\mathcal{I}_s^2(x_1,y_1)+\sin(2k_1\tau)\mathcal{I}_c(x_1,y_1)\mathcal{I}_s(x_1,y_1)\right],$$

where $\mathcal{A}$ denotes the domain of integration which was described above.

Now we need an observable, so that it would be possible to compare the theoretical prediction to measurable quantities. To do so we define the GW power spectrum $\mathcal{P}_h(k)$ in a similar way to what we did for the scalar power spectrum:

$$\langle h^{(m)}_{\mathbf{k}_1}(\tau) h^{(n)}_{\mathbf{k}_2}(\tau)\rangle = \delta^{(3)}(\mathbf{k}_1+\mathbf{k}_2)\delta^{(m)(n)}\frac{2\pi^2}{k_1^3}\mathcal{P}_h(\tau,k),$$

which can be extracted from the two-point function we just computed:

$$\mathcal{P}_h(\tau,k) = \frac{4}{81}\frac{1}{k_1^2\tau^2}\iint_{\mathcal{A}} \mathrm{d}x\mathrm{d}y \frac{x^2}{y^2}\left[1-\frac{(1+x^2-y^2)^2}{4x^2}\right]^2 \mathcal{P}_\zeta(k_1 x)\mathcal{P}_\zeta(k_1 y)\cdot ...$$
$$... \cdot \left[\cos^2(k_1\tau)\mathcal{I}_c^2(x_1,y_1)+\sin^2(k_1\tau)\mathcal{I}_s^2(x_1,y_1)+\sin(2k_1\tau)\mathcal{I}_c(x_1,y_1)\mathcal{I}_s(x_1,y_1)\right].$$

This power spectrum is used to compute the density parameter of gravitational waves. The energy density of GWs is given by [14]:

$$\rho_{GW}(\tau,\mathbf{x}) = \frac{1}{128\pi a(\tau)^2}\left\langle \frac{1}{2}\overline{(h'_{ij})^2}+\frac{1}{2}\overline{(\nabla h_{ij})^2}\right\rangle \approx \frac{1}{128\pi a(\tau)^2}\left\langle \overline{(\nabla h_{ij})^2}\right\rangle,$$

which can be written in terms of the energy density per logarithmic interval of k as:

$$\rho_{GW}(\tau) = \int \mathrm{d}\log k\ \rho_{GW}(\tau,k),\ \ \rho_{GW}(\tau,k) = \frac{1}{64\pi}\left(\frac{k}{a(\tau)}\right)^2 \overline{\mathcal{P}_h(\tau,k)}.$$

We then define the energy density parameter of GWs as:

$$\Omega_{GW}(\tau,k) := \frac{\rho_{GW}(\tau,k)}{\rho_{critical}} = \frac{1}{24}\left(\frac{k}{\mathcal{H}(\tau)}\right)^2 \overline{\mathcal{P}_h(\tau,k)},\ \ \rho_{critical} = \frac{3H^2}{8\pi},$$

where the bar denotes an average over time. Since this is the quantity that we want to compare with the experimental results we want to compute it at present time. This can be done performing a rescaling using the scale factor through the different epochs and relating the radiation density during the radiation dominated era to the current one at time τ_0 through entropy conservation. Finally, after performing the average over the conformal time τ and the coordinate change from (x,y) to (s,d) that we defined above, the density parameter of gravitational waves reads:

$$\Omega_{GW}(\tau_0,k) = \frac{c_g\Omega_{r,0}}{36}\int_{1/\sqrt{3}}^{\infty}\mathrm{d}s\int_0^{1/\sqrt{3}}\mathrm{d}d\left[\frac{(s^2-1/3)(d^2-1/3)}{s^2-d^2}\right]^2\cdot ...$$

$$... \cdot \mathcal{P}_\zeta\left(\frac{k\sqrt{3}}{2}(s+d)\right)\mathcal{P}_\zeta\left(\frac{k\sqrt{3}}{2}(s-d)\right)\left[\mathcal{I}_c^2(s,d)+\mathcal{I}_s^2(s,d)\right], \tag{4.3}$$

where $c_g \approx 0.4$ is a function of the relativistic degrees of freedom, $\Omega_{r,0} \approx 8 \cdot 10^{-5}$ is the present value for the radiation density while $\mathcal{P}_\zeta$ is the scalar power spectrum. The two functions $\mathcal{I}_c$ and $\mathcal{I}_s$ come from the analytic integration of the transfer function and read:

$$\mathcal{I}_c(s,d) = -36\pi\frac{(s^2+d^2-2)^2}{(s^2-d^2)^3}\theta(s-1),$$

$$\mathcal{I}_s(s,d) = -36\frac{s^2+d^2-2}{(s^2-d^2)^2}\left[\frac{s^2+d^2-2}{s^2-d^2}\log\left(\frac{1-d^2}{|s^2-1|}\right)+2\right].$$

4.1.1 Some examples

In the following we will present some examples of analytical and numerical computations for some power spectra.

δ function We consider the following power spectrum:

$$\mathcal{P}_\zeta^\delta(p) = \mathcal{A}^2\delta\left(\log\frac{p}{k_p}\right) = k_p\mathcal{A}^2\delta(p-k_p),$$

where k_p is the peak frequency. We can then insert the power spectrum into the expression for the density parameter:

$$\Omega_{GW}^\delta(\tau_0,k) = \frac{c_g\Omega_{r,0}k_p^2\mathcal{A}^4}{36}\int_{1/\sqrt{3}}^\infty \mathrm{d}s\int_0^{1/\sqrt{3}}\mathrm{d}d\left[\frac{(s^2-1/3)(d^2-1/3)}{s^2-d^2}\right]^2\cdot ...$$

$$... \cdot \delta\left(\frac{k\sqrt{3}}{2}(s+d)-k_p\right)\delta\left(\frac{k\sqrt{3}}{2}(s-d)-k_p\right)\left[\mathcal{I}_c^2(s,d)+\mathcal{I}_s^2(s,d)\right] =$$

$$\frac{c_g\Omega_{r,0}k_p^2\mathcal{A}^4}{36}\int_{1/\sqrt{3}}^\infty \mathrm{d}s\int_0^{1/\sqrt{3}}\mathrm{d}d\left[\frac{(s^2-1/3)(d^2-1/3)}{s^2-d^2}\right]^2\cdot ...$$

$$... \cdot \delta\left(\frac{k\sqrt{3}}{2}\left(s+d-\frac{2k_p}{\sqrt{3}k}\right)\right)\delta\left(\frac{k\sqrt{3}}{2}\left(s-d-\frac{2k_p}{\sqrt{3}k}\right)\right)\left[\mathcal{I}_c^2(s,d)+\mathcal{I}_s^2(s,d)\right].$$

Since $\delta(ax) = |a|^{-1}\delta(x)$ we have:

$$\Omega_{GW}^\delta(\tau_0,k) = \frac{c_g\Omega_{r,0}k_p^2\mathcal{A}^4}{36}\frac{4}{3k^2}\int_{1/\sqrt{3}}^\infty \mathrm{d}s\int_0^{1/\sqrt{3}}\mathrm{d}d\left[\frac{(s^2-1/3)(d^2-1/3)}{s^2-d^2}\right]^2\cdot ...$$

$$... \cdot \delta\left(s+d-\frac{2k_p}{\sqrt{3}k}\right)\delta\left(s-d-\frac{2k_p}{\sqrt{3}k}\right)\left[\mathcal{I}_c^2(s,d)+\mathcal{I}_s^2(s,d)\right].$$

We can perform the integral over d assuming that the 0 of the δ enters the integration domain (we will see later that this assumption is correct) and get:

$$\Omega^{\delta}_{GW}(\tau_0,k)=\frac{c_g\Omega_{r,0}k_p^2\mathcal{A}^4}{36}\frac{4}{3k^2}\int_{1/\sqrt{3}}^{\infty}\mathrm{d}s\int_0^{1/\sqrt{3}}\mathrm{d}d\left[\frac{(s^2-1/3)(d^2-1/3)}{s^2-d^2}\right]^2\cdot\ldots$$

$$\ldots\cdot\delta\left(s+d-\frac{2k_p}{\sqrt{3}k}\right)\delta\left(d-\left(s-\frac{2k_p}{\sqrt{3}k}\right)\right)\left[\mathcal{I}_c^2(s,d)+\mathcal{I}_s^2(s,d)\right]=$$

$$\frac{c_g\Omega_{r,0}k_p^2\mathcal{A}^4}{36}\frac{4}{3k^2}\int_{1/\sqrt{3}}^{\infty}\mathrm{d}s\left[\frac{(s^2-1/3)\left(\left(s-\frac{2k_p}{\sqrt{3}k}\right)^2-1/3\right)}{s^2-\left(s-\frac{2k_p}{\sqrt{3}k}\right)^2}\right]^2\cdot\ldots$$

$$\ldots\cdot\delta\left(2s-\frac{4k_p}{\sqrt{3}k}\right)\left[\mathcal{I}_c^2\left(s,s-\frac{2k_p}{\sqrt{3}k}\right)+\mathcal{I}_s^2\left(s,s-\frac{2k_p}{\sqrt{3}k}\right)\right].$$

Exploiting again the fact that $\delta(ax)=|a|^{-1}\delta(x)$ and assuming that the 0 of the δ enters the integration domain we can integrate over s to obtain:

$$\Omega^{\delta}_{GW}(\tau_0,k)=\frac{c_g\Omega_{r,0}\mathcal{A}^4}{486}\left(\frac{k_p}{k}\right)^2\left(1-\frac{k^2}{4k_p^2}\right)^2\left[\mathcal{I}_c^2\left(\frac{2k_p}{\sqrt{3}k},0\right)+\mathcal{I}_s^2\left(\frac{2k_p}{\sqrt{3}k},0\right)\right].$$

This corresponds to having $d=0$ and $s=2k_p/(\sqrt{3}k)$. $d=0$ is within the domain of integration, while $s=2k_p/(\sqrt{3}k)$ is within the domain of integration only if $k<2k_p$. This is a general condition for the wave number of secondary GWs, which states that GWs with wave number $k<Nk_p$ are produced at N-th order, while the effects of GWs with $k>Nk_p$ are much suppressed [20]. The final result can then be written as:

$$\Omega^{\delta}_{GW}(\tau_0,k)=\frac{c_g\Omega_{r,0}\mathcal{A}^4}{486}\left(\frac{k_p}{k}\right)^2\left(1-\frac{k^2}{4k_p^2}\right)^2\left[\mathcal{I}_c^2\left(\frac{2k_p}{\sqrt{3}k},0\right)+\mathcal{I}_s^2\left(\frac{2k_p}{\sqrt{3}k},0\right)\right]\theta\left(1-\frac{k}{2k_p}\right).$$

This is shown in figure (4.1).

Top-hat function This power spectrum is given by:

$$\mathcal{P}_\zeta^{\mathrm{TH}}(p)=\begin{cases}\dfrac{\mathcal{A}^2}{2\Delta} & \text{for } |\log(p/k_p)|<\Delta\\ 0 & \text{otherwise}\end{cases}$$

and its limit $\Delta\to 0$ reproduces the δ function power spectrum. This was analysed in [20].

With some suitable changes of coordinates it is possible to write the energy density parameter as:

$$\Omega^{TH}_{GW}(\tau_0,k)=\left(\frac{1}{2\Delta}\right)^2\iint_{\mathcal{D}_1\cap\mathcal{D}_2}\mathrm{d}\log p\ \mathrm{d}\delta\ \mathcal{J}(p/k,\delta)w(p/k,\delta,\tau_0)\Omega^{\delta}_{GW}(\tau_0,k/p),$$

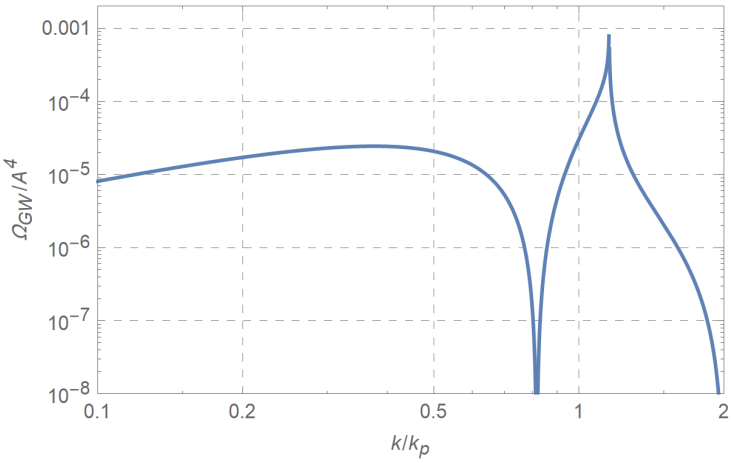

Figure 4.1: Energy density parameter for a δ function scalar power spectrum.

where we have defined the functions:

$$\mathcal{J}(p/k,\delta) := \frac{k}{p}\left[1-\delta^2\left(\frac{k}{2p}\right)^2\right]^{-1},$$

$$w(p/k,\delta,\tau) := (1-\delta^2)^2\left[1-\delta^2\left(\frac{k}{2p}\right)^2\right]^{-1}\left[\frac{I(k,p+k\delta/2,p-k\delta/2,\tau)}{I(k,p,p,\tau)}\right]^2,$$

$$I(k,k_1,k_2,\tau) := k\int_0^\tau \mathrm{d}\tilde{\tau}a(\tilde{\tau})g_{\mathbf{k}}(\tau,\tilde{\tau})f(\tau,k_1,k_2),$$

where $g_{\mathbf{k}}$ is the Green function defined in Eq. (4.1) and f is the same function defined in Eq. (4.2). The domain of integration is instead given by:

$$\mathcal{D}_1 := \{|\delta|<1, p>k/2\},\ \mathcal{D}_2 = \{|\log[(p+k\delta/2)/k_p]|<\Delta, |\log[(p-k\delta/2)/k_p]|<\Delta\}.$$

In figure (4.2) we show the plot of Ω_{GW}^{TH} for different values of Δ and $\Omega_{GW}^{TH}/\Omega_{GW}^{\delta}$ at $k=k_p$ as a function of Δ.

From the left panel we actually see that the limit $\Delta\to 0$ corresponds to the case of a δ function power spectrum. Also for small Δ it is almost the same at least qualitatively, while for $\Delta = 1.0$ it changes its behaviour. It exhibits a flat plateau over the region $|\log(k/k_p)|<\Delta$, reflecting the behaviour of the scalar modes. The $\mathcal{O}(10^4)$ difference in scale between this plot and the one in figure (4.1) is due to the normalization, in fact in [20] there is an extra factor $\Omega_{r,0}^{-1}$ in the plot.

From the right panel we see that for small Δ, in particular $\Delta<0.1$, $\Omega_{GW}^{TH}(\tau_0,k=k_p)$ as a function of Δ is almost constant and can also be approximated by Ω_{GW}^{δ}. Also we see that it decreases as Δ^{-2} for large Δ, which is a behaviour that is expected any generic peaked power spectrum.

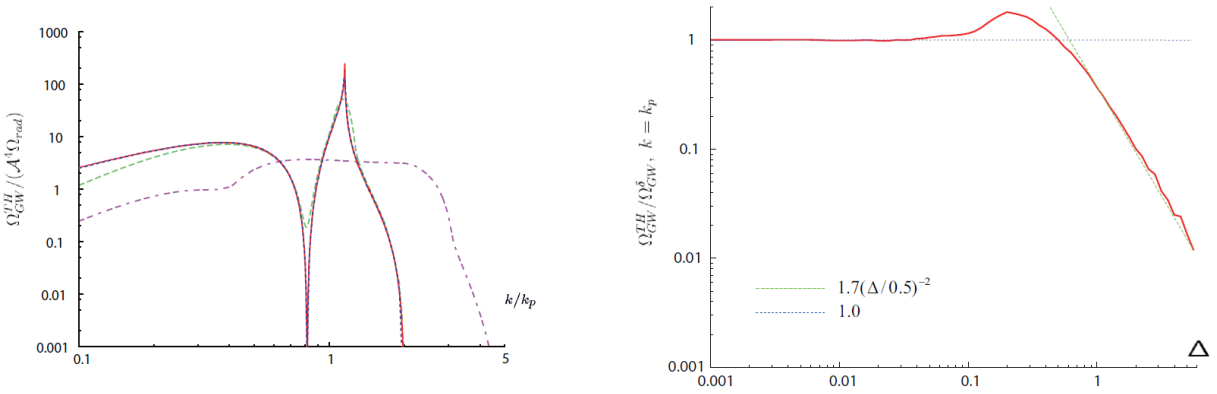

Figure 4.2: Left panel: normalized energy density parameter for a top-hat function scalar power spectrum. The red line corresponds to the $\Delta \to 0$ limit, the blue one corresponds to $\Delta = 10^{-3}$, the green one corresponds to $\Delta = 10^{-1}$, the purple one correspond to $\Delta = 1$. **Right panel**: ratio $\Omega_{GW}^{TH}/\Omega_{GW}^{\delta}$ at $k = k_p$ as a function of Δ. The green line corresponds to the Δ^{-2} fit. Source: [20].

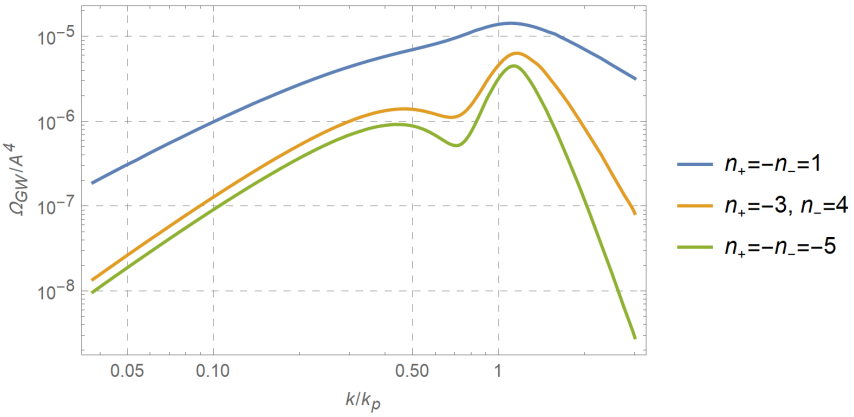

Figure 4.3: Energy density parameter for a broken power law scalar power spectrum for three different sets of exponents.

Broken power law In this case the power spectrum is given by:

$$\mathcal{P}_\zeta^{BPL}(p) = \mathcal{A}^2 \left[\left(\frac{p}{k_p}\right)^{n_+} \theta(p-k_p) + \left(\frac{p}{k_p}\right)^{n_-} \theta(k_p - p) \right], \tag{4.4}$$

where θ is the Heaviside step function and in general one has $n_+ < 0$, $n_- > 0$. The details of the computation of the energy density parameter are given in Appendix A. In figure (4.3) we show the numerical result for three different sets of exponents, i.e. $(n_+, n_-) = (-1, 1), (-3, 4), (-5, 5)$. We see that as the modulus of the exponents increases the shape of the energy density parameter resembles the one for the case of the δ function power spectrum. This is due to the fact that the peak in the power spectrum becomes steeper and steeper and peaked at $k = k_p$. Note that the limit $n_\pm \to \mp\infty$ does not correspond to a δ function, but it is interesting to note this similarity.

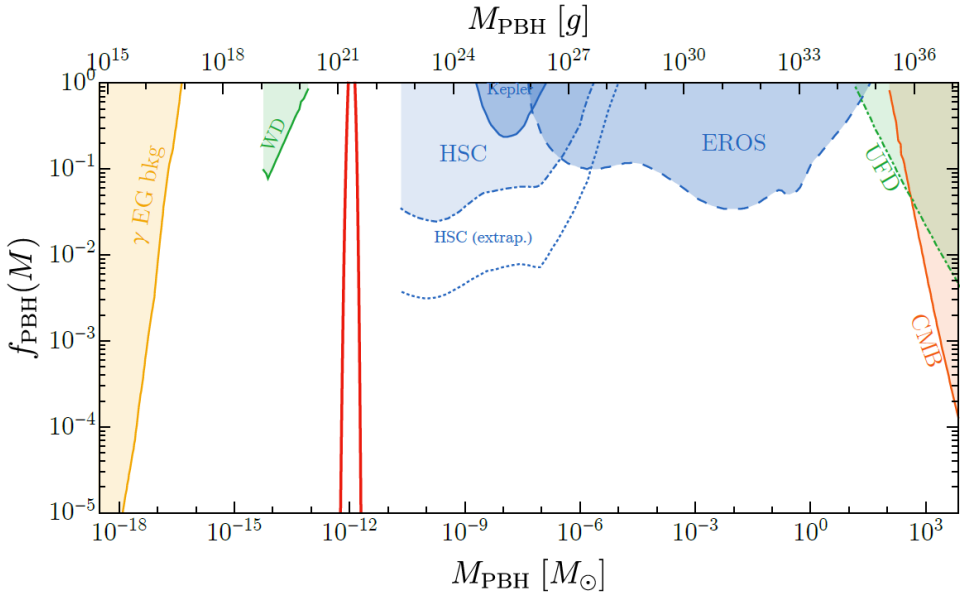

Figure 4.4: Observational constraints on the abundance of PBH dark matter. Source: [26].

4.2 Current observational bounds

We show the current observational bounds on the abundance of PBH Dark Matter in figure (4.4) [26]. The thick red line corresponds to PBHs formed from a monochromatic power spectrum, i.e. $\mathcal{P}_\zeta(p) = \mathcal{A}^2 k_p \delta(p - k_p)$, peaked at $k_p = 2\pi f_{LISA} = 2\pi \cdot 3.4$ mHz and with $\mathcal{A}^2 = 0.033$. The meanings of every line are given here:

- γ EG bkg: extra-galactic gamma rays as black hole evaporation [27];
- WD: existence of white dwarves in our local galaxy [28];
- HSC: microlensing events on M31 with the Subaru/HSC Andromeda observation [29];
- Kepler: milli/microlensing effect from the Kepler satellite [30];
- EROS: EROS/MACHO microlensing [31];
- UFD: heating of a star cluster in the ultra-faint dwarf galaxy Eridanus II [32];
- CMB: accretion rate and luminosity of PBHs [33][34][35].

We see that in the regions $M_{PBH} \sim [10^{-17} M_\odot, 10^{-14} M_\odot]$ and $M_{PBH} \sim [10^{-13} M_\odot, 10^{-11} M_\odot]$ there are no observational bounds, hence PBHs whose mass belongs in these ranges can account for all of DM. Also the peak frequency of LISA corresponds to $M_{PBH} \sim 10^{-12} M_\odot$, which is not a constrained value for the mass. This is a very lucky serendipity, since if PBHs of this mass are all of DM then LISA would detect the GWs produced during their formation and the signal would be Gaussian, isotropic and unpolarized [26].

The mass of PBHs only depends on the peak scale and not on the particular form of the scalar power spectrum, therefore setting $k_p = 2\pi f_{LISA}$ for all the aforementioned examples will lead to the same conclusion, i.e. there are no constraints in this mass region.

4.3 Interferometry sensitivity curves

In general the signal arriving to a detector can be parametrized as [36]:

$$s(t) = h(t) + n(t),$$

where h is the actual signal while n is the noise. Assuming the latter to be gaussian and with zero mean value we can define the *Power Spectral Density* (PSD) $S_n(f)$ as:

$$\langle \tilde{n}(f)\tilde{n}^*(f')\rangle =: \frac{1}{2}\delta(f-f')S_n(f),$$

where $\tilde{n}(f)$ is the Fourier transformed of the noise. An integration over the positive frequencies gives:

$$\overline{|n(t)|^2} = \int_0^{+\infty} \mathrm{d}f S_n(f),$$

and hence we can define the amplitude spectral density as the square root of the PSD. We then define the dimensionless characteristic strain for the source amplitude, $h_c(f)$, and for the noise, $h_n(f)$, such that the Signal-to-Noise Ratio (SNR) ϱ can be written as:

$$\varrho^2 = \int_{-\infty}^{+\infty} \mathrm{d}\log f \left[\frac{h_c(f)}{h_n(f)}\right]^2.$$

With these definitions we have:

$$\sqrt{S_n(f)} = \frac{1}{\sqrt{f}} h_n(f).$$

We give these definitions because they are among the most plotted ones to show the sensitivities of interferometers. It can be shown that they are related to the energy density parameter of GWs as follows:

$$\Omega_{GW}(\tau_0, f)h^2 = 6\pi^2 f^3 S_n(f) \cdot 10^{34},$$

so that we can make a comparison between our calculations and the sensitivity curves. The number h is defined as $H_0 = 100h$ km s^{-1} Mpc^{-1}, H_0 being the Hubble parameter measured at present time. Its most updated value is $h = 0.721 \pm 0.020$ [37].

The PSDs can be found in the literature. Here we give them for some of the current and future experiments together with their frequency ranges. These are the most updated ones to our knowledge.

- aLIGO, $f \in [5, 5000]$ Hz (source: `https://dcc.ligo.org/LIGO-T1800044/public`). The LIGO collaboration provides the updated files for the characteristic strain (not an analytical fit) after the most recent measurement of coating thermal noise on aLIGO samples.

- LISA, $f \in [10^{-5}, 1]$ Hz [38]:

$$S_n^{\text{LISA}}(f) = \frac{10}{3L^2}\left[P_{OMS}(f) + 2\left(1+\cos^2\left(\frac{f}{f_*}\right)\right)\frac{P_{acc}(f)}{(2\pi f^4)}\right]\left[1+\frac{3}{5}\left(\frac{f}{f_*}\right)\right],$$

  where $L = 2.5$ Gm is the length of the arms, $f_* = c/(2\pi L) = 19.09$ mHz and the so-called Optical Metrology Noise P_{OMS} and the test mass Acceleration noise P_{acc} are given by:

$$P_{OMS}(f) = 2.25 \cdot 10^{-22}\ \text{m}^2\left[1+\left(\frac{2\ \text{mHz}}{f}\right)^2\right]\ \text{Hz}^{-1},$$

$$P_{acc}(f) = 9 \cdot 10^{-30}\ \text{m}^2\text{s}^{-4}\left[1+\left(\frac{0.4\ \text{mHz}}{f}\right)^2\right]\left[1+\left(\frac{8\ \text{mHz}}{f}\right)^4\right]\ \text{Hz}^{-1}.$$

- DECIGO, $f \in [10^{-5}, 100]$ Hz [39]:

$$S_n^{\text{DECIGO}}(f) = 7.05 \cdot 10^{-48}\left[1+\left(\frac{f}{f_p}\right)^2\right] + 4.8 \cdot 10^{-51}\left(\frac{f}{1\ \text{Hz}}\right)^{-4}\frac{1}{1+\left(\frac{f}{f_p}\right)^2} + ...$$

$$... + 5.33 \cdot 10^{-52}\left(\frac{f}{1\ \text{Hz}}\right)^{-4}\ \text{Hz}^{-1},$$

  where $f_p = 7.36$ Hz.

- BBO, $f \in [10^{-5}, 100]$ Hz [39]:

$$S_n^{\text{BBO}}(f) = 2 \cdot 10^{-49}\left(\frac{f}{1\ \text{Hz}}\right)^2 + 4.58 \cdot 10^{-49} + 1.26 \cdot 10^{-51}\left(\frac{f}{1\ \text{Hz}}\right)^{-4}\ \text{Hz}^{-1}.$$

- MAGIS-100 and MAGIS-km, $f \in [0.1, 10]$ Hz [40][41]. For the MAGIS-100 experiment two curves are reported: the one denoted by "MAGIS-100 (5 year)" shows what is possible after sensor research and development, the one denoted by "MAGIS-km" is the estimated sensitivity of a future km-scale experiment. The two strains are given by:

$$S_n^{\text{MAGIS-100 (5 year)}}(f) = 10^{-38}\ \text{Hz}^{-1},\ S_n^{\text{MAGIS-km}}(f) = 10^{-42}\ \text{Hz}^{-1}.$$

- ET , $f \in [1, 10^4]$ Hz [42]:

$$S_n^{\text{ET}}(f) = S_0\left[x^\alpha + a_0 x^\beta + \frac{b_0(1+b_1x+b_2x^2+b_3x^3+b_4x_4+b_5x^5+b_6x^6)}{1+c_1x+c_2x^2+c_3x^3+c_4x^4}\right],$$

  where $x = f/(200\ \text{Hz})$, $S_0 = 1.52 \cdot 10^{-52}$, $\alpha = -4.1$, $\beta = -0.69$, $a_0 = 186$, $b_0 = 233$, $b_1 = 31$, $b_2 = -65, b_3 = 52$, $b_4 = -42, b_5 = 10$, $b_6 = 12$, $c_1 = 14, c_2 = -37$, $c_3 = 19$ and $c_4 = 27$.

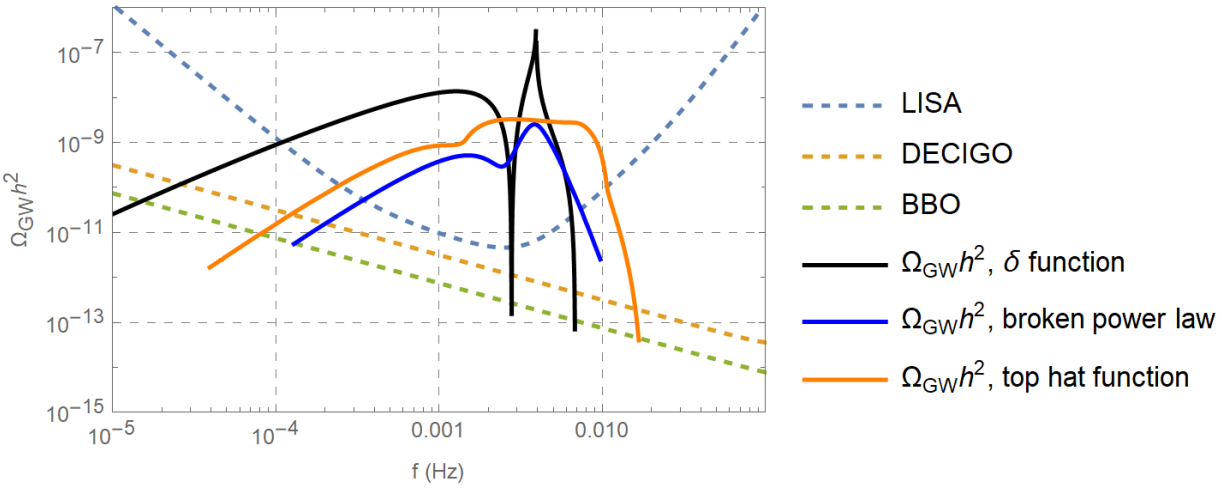

Figure 4.5: Comparison between the energy density parameters computed from a δ function, top hat function and broken power law scalar power spectrum with the interferometry sensitivity curves.

We compare the examples we studied in section 4.1.1 (for the case of broken power law we consider $n_+ = -n_- = -5$), considering $\mathcal{A}^2 = 0.033$ and a peak scale $k_p = 2\pi f_{LISA}$. The energy density parameter is multiplied by a factor h^2 by convention. The comparison is shown in figure (4.5). We see that the models considered in the examples produce a GW signal that enter the frequency ranges of LISA, DECIGO and BBO. For the other interferometers these signals would be out of their frequency range: this would mean relying on higher frequency GWs, which would have been produced by lower mass PBHs, namely around $M_{PBH} \sim 10^{-18} M_\odot$ or even less. However these values of the mass are very constrained, actually it is very improbable that PBHs of these masses can account for a significant fraction of DM, see the observational bounds from extra-galactic gamma rays in figure (4.4). We then conclude that it is very unlikely that these interferometers will be able to detect the GW background generated by PBH production.

Chapter 5

GWs from Fibre Inflation

In this chapter we present the inflationary model of Fibre Inflation and we show how we can achieve the formation of primordial black holes. We then present the original work of this thesis, namely the study of gravitational wave production after PBH formation, comparing our results with the current observational bounds and the interferometry sensitivities.

5.1 Fibre Inflation

Fibre Inflation [43] is an inflationary model derived from string theory in the context of type IIB flux compactification, and which we will consider in the next sections to study secondary GW production.

The reason why we consider this framework is because in type IIB string theory it is possible to achieve moduli stabilisation and to obtain an effective 10D supergravity action with $\mathcal{N} = 1$ supersymmetry, which allows for chiral matter. After compactification on a Calabi-Yau (CY) manifold (a three-fold to be precise) the $\mathcal{N} = 1$ supersymmetry is preserved, hence it is possible to compare results with observations. The moduli in the 4D supergravity action are called Kähler moduli and they are complex scalar fields that parametrize geometrical features of the CY manifold such as its volume and the deformations of the extra dimensions. We can parametrize them as $T_i = \tau_i + ib_i,\ i = 1, ..., h_{1,1}(X)$, where $h_{1,1}(X)$ is a Hodge number of the CY manifold X. In terms of the real part of the Kähler moduli τ_i we can write the volume of the CY manifold as:

$$\mathcal{V} = t_{\mathbb{P}^1}\tau_{K3} - \tau_{dP}^{3/2},$$

where $t_{\mathbb{P}^1}$ is the volume of the $\mathbb{P}^1$ base on which a K3 divisor with volume τ_{K3} is fibred and τ_{dP} is the volume of a diagonal del Pezzo divisor. It is shown that in a $1/\mathcal{V} \ll 1$ expansion only $\mathcal{V}$ and τ_{dP} are lifted by non-perturbative corrections to the superpotential W and perturbative α' corrections to the Kähler potential K, while τ_{K3} remains flat and so it represents a good candidate for the inflaton since it enjoys an effective non-compact rescale symmetry.

Considering open-string loop corrections and higher derivative α' effects one obtains an

	C_W	A_W	B_W	$G_W/\langle\mathcal{V}\rangle$	$R_W/\langle\mathcal{V}\rangle$	$\langle\tau_{K3}\rangle$	$\langle\mathcal{V}\rangle$
$\mathcal{P}_1$	1/10	2/100	1	1.303386×10^{-3}	6.58724×10^{-3}	3.89	107.3
$\mathcal{P}_2$	4/100	2/100	1	3.080548×10^{-5}	7.071067×10^{-4}	14.30	1000
$\mathcal{P}_3$	1.978/100	1.65/100	1.01	9.257715×10^{-8}	1.414×10^{-5}	168.03	50000

Table 5.1: Examples of parameters for the Fibre Inflation potential Eq. (5.2) that allow for PBH formation of mass $10^{-14}M_\odot$. In all cases $D_W = 0$.

inflationary potential for τ_{K3} of the form:

$$V_{inf}(\tau_{K3}) = \left(\frac{C_{up}}{\mathcal{V}^{4/3}} + g_s^2\frac{C_{KK}}{\tau_{K3}^2} + \frac{W_0^2}{\sqrt{g_s}}\frac{\epsilon_{F^4}}{\mathcal{V}\tau_{K3}} + \frac{C_W}{\mathcal{V}\sqrt{\tau_{K3}}} + g_s^2 D_{KK}\frac{\tau_{K3}}{\mathcal{V}^2} + \delta_{F^4}\frac{W_0^2}{\sqrt{g_s}}\frac{\sqrt{\tau_{K3}}}{\mathcal{V}^2}\right)\frac{W_0^2}{\mathcal{V}^2},$$

where $g_s \ll 1$ is the string coupling, $W_0 = \mathcal{O}(1-10)$ is the superpotential (which is constant after moduli stabilisation), C_{up} controls the uplifting contribution and depends on $\mathcal{V}$, C_{KK}, D_{KK} and C_W are coefficients for the 1-loop open string corrections while ϵ_{F^4} and δ_{F^4} are coefficients for the higher derivatives $\alpha'\,F^4$ effects.

In order to generate a potential that can allow for PBH formation we need to introduce some other corrections. In particular C_W is not a constant but it is a function of the modulus τ_{K3} of the following form:

$$C_W(\tau_{K3}) = C_W - \frac{A_W\sqrt{\tau_{K3}}}{\sqrt{\tau_{K3}} - B_W},$$

where A_W, B_W and C_W are constant parameters. Also there is another 1-loop correction to the effective action which is crucial for the formation of PBHs given by:

$$\delta V_W = W_0^2\frac{\tau_{K3}}{\mathcal{V}^4}\left(D_W - \frac{G_W}{1 + R_W\frac{\tau_{K3}^{3/2}}{\mathcal{V}}}\right),$$

where again D_W, G_W and R_W are constant parameters. In Fibre Inflation models many contributions to the inflaton potential can be neglected such as the Kaluza-Klein loop correction, so that $C_{KK} = D_{KK} = 0$. We will also neglect the higher derivative effects, so the inflaton potential we will consider is given by:

$$V_{inf}(\tau_{K3}) = \frac{W_0^2}{\mathcal{V}^3}\left[\frac{C_{up}}{\mathcal{V}^{1/3}} - \frac{C_W}{\sqrt{\tau_{K3}}} + \frac{A_W}{\sqrt{\tau_{K3}} - B_W} + \frac{\tau_{K3}}{\mathcal{V}}\left(D_W - \frac{G_W}{1 + R_W\frac{\tau_{K3}^{3/2}}{\mathcal{V}}}\right)\right]. \quad (5.1)$$

We can express this potential in terms of the canonically normalized inflaton field ϕ, defined as:

$$\phi := \frac{\sqrt{3}}{2}\log\langle\tau_{K3}\rangle + \hat{\phi},$$

where $\langle\tau_{K3}\rangle$ is the minimum of the modulus τ_{K3}. Then the potential becomes:

$$V_{inf}(\phi) = V_0\left[C_1 - e^{-\hat{\phi}/\sqrt{3}}\left(1 - \frac{C_2}{1 - C_3e^{-\hat{\phi}/\sqrt{3}}}\right) + C_4e^{2\hat{\phi}/\sqrt{3}}\left(1 - \frac{C_5}{1 + C_6e^{\hat{\phi}\sqrt{3}}}\right)\right], \quad (5.2)$$

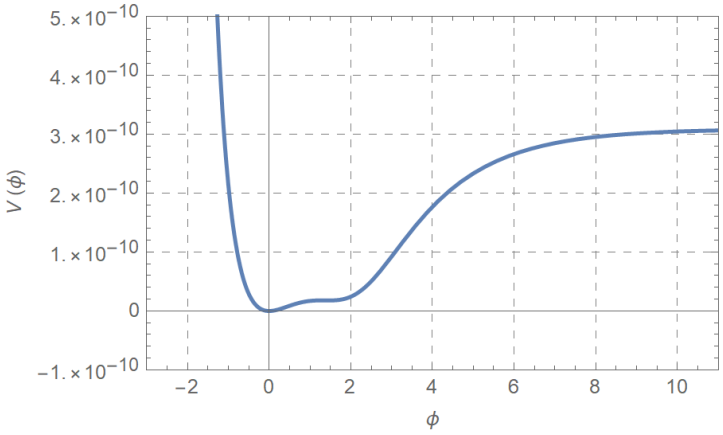

Figure 5.1: Fibre Inflation potential corresponding to the set of parameters $\mathcal{P}_2$ in table (5.1)

where:

$$V_0 = \frac{C_W W_0^2}{\mathcal{V}^{10/3}},\ C_1 = \frac{C_{up}\langle\tau_{K3}\rangle^{1/2}}{C_W\mathcal{V}^{1/3}},\ C_2 = \frac{A_W}{C_W},\ C_3 = \frac{B_W}{\langle\tau_{K3}\rangle^{1/2}},$$
$$C_4 = \frac{\langle\tau_{K3}\rangle^{3/2}D_W}{\mathcal{V}C_W},\ C_5 = \frac{G_W}{D_W},\ C_6 = \frac{\langle\tau_{K3}\rangle^{3/2}R_W}{\mathcal{V}}.$$

In figure (5.1) we show the Fibre Inflation potential Eq. (5.2) for the set of parameters $\mathcal{P}_2$ of table (5.1).

From Fibre Inflation it is then possible to compute the Hubble parameter H and the slow roll parameters, which are shown in the figure (5.2). This was done solving the Friedmann equation (2.12) and the inflaton equation of motion (3.2) simultaneously as functions of the number of efoldings N, which are the following:

$$H' + \frac{1}{2}H(\phi')^2 = 0,\ H^2\phi'' + (HH' + 3H^2)\phi' + \frac{\delta V[\phi]}{\delta\phi} = 0, \tag{5.3}$$

where in this case the prime $'$ denotes a derivation with respect to N. The slow roll parameters were then computed as:

$$\epsilon = -\frac{H'}{H},\ \eta = 2\epsilon - \frac{2}{H^2(\phi')^2}\frac{\delta V[\phi]}{\delta\phi} - 6$$

5.1.1 PBH formation in Fibre Inflation

The primordial power spectrum is computed solving the MS equation (3.12) since we cannot consider slow roll approximations Eq. (3.21) when modes corresponding to about $N \in [15, 25]$ efoldings before the end of inflation enter the Hubble horizon. The MS equation as a function of N reads:

$$u_k'' + (1-\epsilon)u_k' + \left[\left(\frac{k}{aH}\right)^2 + \left(1+\frac{\eta}{2}\right)\left(\epsilon - \frac{\eta}{2} - 2\right) - \frac{\eta'}{2}\right]u_k = 0,$$

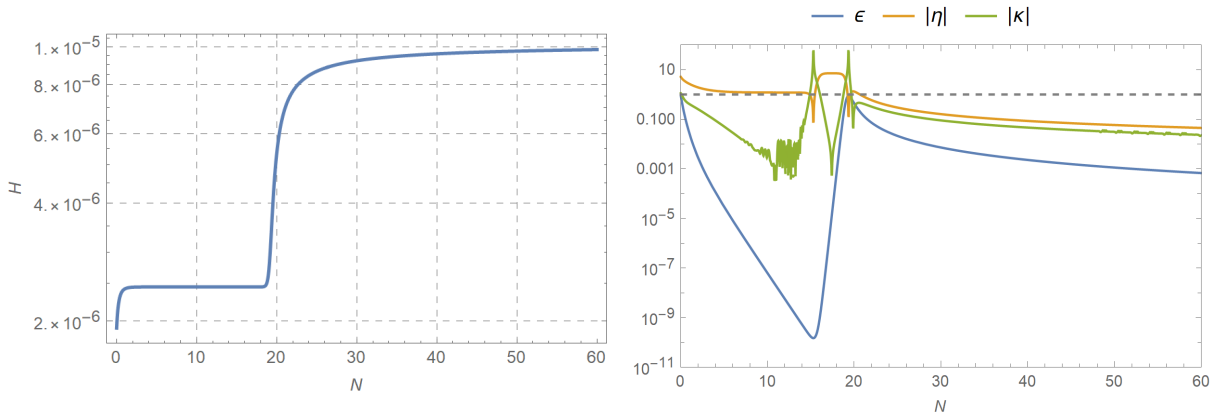

Figure 5.2: Left panel: the Hubble parameter H as a function of the number of efoldings before the end of inflation. **Right panel**: the Hubble slow roll parameters ϵ, η and κ derived from the Fibre Inflation potential Eq. (5.1), the Friedmann equation and the inflaton equation of motion Eqs. (5.3).

where the prime $'$ denotes a derivation with respect to N and it has been used the identity:

$$\frac{1}{z}\frac{\mathrm{d}^2 z}{\mathrm{d}\tau^2} = (aH)^2\left[2-\epsilon+\frac{3\eta}{2}-\frac{\epsilon\eta}{2}+\frac{\eta^2}{4}+\frac{\eta\kappa}{2}\right]$$

to rewrite the effective mass of the curvature perturbations. The dimensionless power spectrum is given by:

$$\mathcal{P}_u(k) = \frac{k^3}{2\pi^2}\left|\frac{u_k}{z}\right|^2,$$

which in the superhorizon limit $k\tau \to 0$ can be approximated as:

$$\mathcal{P}_{u,sh}(k) = \frac{H^2}{8\pi^2\epsilon}\frac{2^{2\nu-1}|\Gamma(\nu)|^2}{\pi}\left(\frac{k}{aH}\right)^{3-2\nu}$$

In the slow roll regime $\epsilon, \eta, \kappa \ll 1$ we can approximate $z''/z \approx 2(2+3\epsilon+3\eta)/\tau^2$ so that $\nu \approx 3/2+\epsilon+\eta/2$ and the power spectrum can be computed at horizon crossing as:

$$\mathcal{P}_{u,sr}(k) = \left.\frac{H^2}{8\pi^2\epsilon}\right|_{k=aH}. \tag{5.4}$$

To compute the power spectrum the MS equation (3.12) is solved numerically and the curvature perturbations u_k and the function z are evaluated at the end of inflation. In figure (5.3) we show the result with a comparison with the slow roll approximation. As we see it breaks down when the inflaton field approaches the point of inflection of the potential and the constant roll phase is reached: this is indeed the moment when the curvature perturbations are enhanced and PBH formation can be achieved.

The spectral index can be computed and with the set of the parameters $\mathcal{P}_2$ in table (5.1) turns out to be $n_s = 0.9437$. This is 3σ redder than the current best fit, however the tension can be decreased including non-zero neutrino masses, making the result compatible within 2σ.

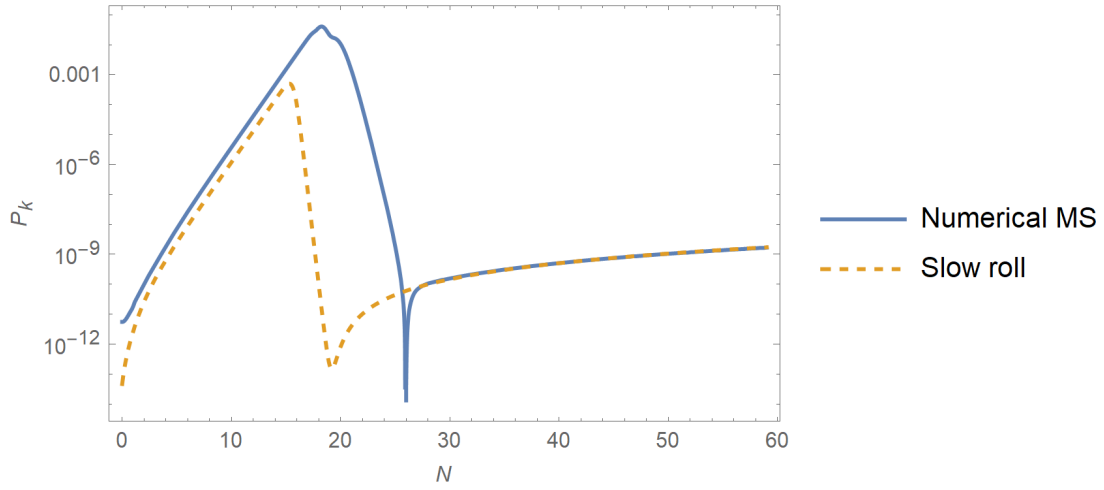

Figure 5.3: The thick blue line represents the primordial power spectrum in Fibre Inflation obtained with the inflaton potential Eq. (5.2) with the set of parameters $\mathcal{P}_2$ in table (5.1). The dashed orange line represents the slow roll approximation Eq. (5.4).

5.2 GW production in Fibre Inflation

In this section we compute the energy density parameter of GWs using the Fibre Inflation power spectrum in figure (5.3): this is done applying the theory of secondary GWs we studied in the first section. We will then compare our results with the current observational bounds and the interferometry sensitivities.

Before proceeding we need to make some comments about the code we used to compute the energy density parameter of GWs.

First of all we computed the scalar power spectrum numerically, so it is not defined for all possible values of k, but only for the ones that enter the horizon before the end of inflation, i.e. when $\epsilon < 1$. In particular we have the following interval for the wave number:

$$k \in [1.32 \times 10^{-5}, 2.3 \times 10^{20}].$$

The upper extreme of integration for the variable s is $+\infty$, so in principle the potential should be defined for all possible wave numbers in order for the integration to make sense. Since this does not hold there was the need of fixing the upper extreme of integration. In particular the following condition was adopted:

$$\frac{k\sqrt{3}}{2}\left(s_{max} + d_{max}(= 1/\sqrt{3})\right) = k_{max} \Longrightarrow s_{max} = \frac{1}{\sqrt{3}}\left(\frac{2k_{max}}{k} - 1\right),$$

where k_{max} is the last value at which the scalar power spectrum is defined. This holds because from Eq. (4.3) we see that this is the highest possible value for which the power spectrum in the integrand is defined.

The extremes of integration include the point $s = d = 1/\sqrt{3}$: this would mean that the potential should be defined also for $k = 0$ since in the integrand it appears as a function of

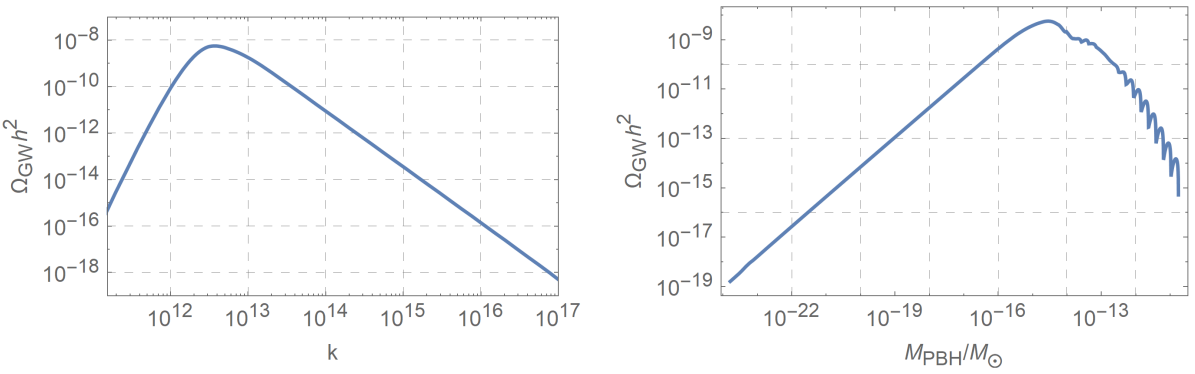

Figure 5.4: Left panel: energy density parameter $\Omega_{GW}h^2$ computed using the Fibre Inflation primordial power spectrum figure (5.3) as a function of the scale k. **Right panel**: energy density parameter $\Omega_{GW}h^2$ computed using the Fibre Inflation primordial power spectrum figure (5.3) as a function of the PBH mass M_{PBH}.

$const \cdot (s-d)$. However the extrapolation of the potential to small values of k performed by the software leads to a decrease of $\mathcal{P}_\zeta$, so there is no need of fixing the lower extreme of integration since it would lead to a negligible contribution to the overall result.

Also it is important to consider the behaviour of the function $\mathcal{I}_c^2(s,d)+\mathcal{I}_s^2(s,d)$ when we change the upper extreme of integration. In fact if we take a look at these functions we see that the dependence on the variable d is weak while for $s \sim \mathcal{O}(10^{3-4})$ its contribution to the integral becomes negligible. This corresponds to a maximum value for the scale of order $k \sim 10^{16-17}$: for higher scales the upper extreme of integration could be too low to actually include the main contribution of this function to the integral and so the results may not be reliable for these values. However as we shall see from our results the energy density parameter corresponding to these scales is already out of reach of current experiments, therefore these scales will not be relevant in the comparison with observations.

Once we computed the energy density parameter we plotted it as a function of the scale k and the PBH mass M, which is computed inverting Eq. (3.30). In particular we have:

$$\frac{M}{M_\odot} = \gamma \left(\frac{g_{*f}}{g_{*0}}\right)^{\frac{1}{6}} \exp\left[36.8 - 2\Delta N_{\rm CMB}^{\rm PBH}\right]. \tag{5.5}$$

We used $\gamma = 1$ and only SM physics involved in PBH production, therefore $g_{*f} = 106.75$ and $g_{*0} = 3.36$. In figure (5.4) we plot the energy density parameter as a function of the scale k, $\Omega_{GW}(\tau_0, k)$, and as a function of the PBH mass M_{PBH}, $\Omega_{GW}(\tau_0, M_{PBH})$.

In order to compare our results with the sensitivities of interferometers we plotted the energy density parameter as a function of the GW peak frequency, $\Omega_{GW}(\tau_0, f_{GW})$. To obtain a relation between the PBH mass and the GW frequency we followed [20], according to which:

$$f_{GW} = 0.03 \text{ Hz} \left(\frac{10^{20}\text{g}}{M_{\rm PBH}}\right)^{\frac{1}{2}} \left(\frac{106.75}{g_{*f}}\right)^{\frac{1}{12}},$$

and since PBH are formed in the RD epoch then, assuming that only SM physics is involved

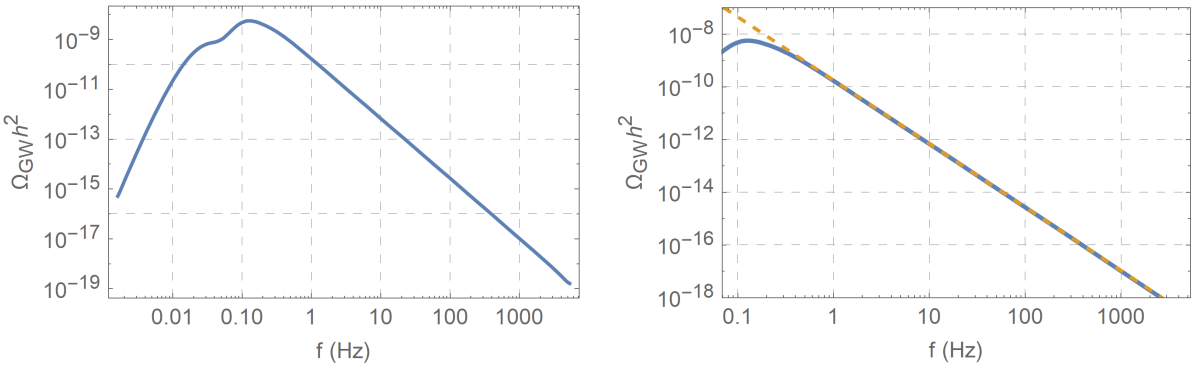

Figure 5.5: Left panel: energy density parameter $\Omega_{GW}h^2$ computed using the Fibre Inflation primordial power spectrum figure (5.3) as a function of the GW peak frequency f_{GW}. **Right panel**: the thick blue line represents the energy density parameter $\Omega_{GW}h^2$ computed using the Fibre Inflation primordial power spectrum figure (5.3) for large scales, while the dashed orange line represents the fit $\Omega_{GW} \sim f^{-2.4}$.

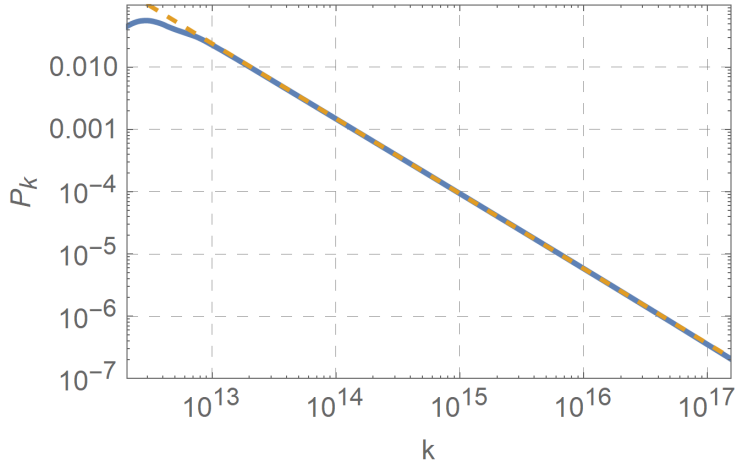

Figure 5.6: The thick blue line represents the primordial power spectrum derived in Fibre Inflation for large scales, while the dashed orange line represents the fit $\mathcal{P}_u \sim k^{-1.2}$

in their production, $g_{*f} = 106.75$ and so:

$$f_{GW} = 0.03 \text{ Hz} \left(\frac{10^{20}\text{g}}{M_{\text{PBH}}}\right)^{\frac{1}{2}} = 6.73 \cdot 10^{-9} \text{ Hz} \left(\frac{M_\odot}{M_{\text{PBH}}}\right)^{\frac{1}{2}}. \tag{5.6}$$

The plot is presented in figure (5.5). We see that the maximum value of the density parameter is reached at a frequency $f_{max} \sim 10^{-1}$ Hz. This suggests that to compare our results with observations we must rely on interferometers that can detect GWs whose frequency is around this value. This is the case for, e.g., LISA, DECIGO, BBO, MAGIS-100, ET and aLIGO; this frequency is out of reach of other possible experiments such as IPTA and SKA whose frequency domain is around $[\sim 10^{-9}, \sim 10^{-6}]$ Hz. For high frequency it was possible to perform a polynomial fit finding $\Omega_{GW}(\tau, f) \sim f^{-2.4}$. This is what we expect since a good fit for the power spectrum for Fibre Inflation is $\mathcal{P}_u(k) \sim k^{-1.2}$ for

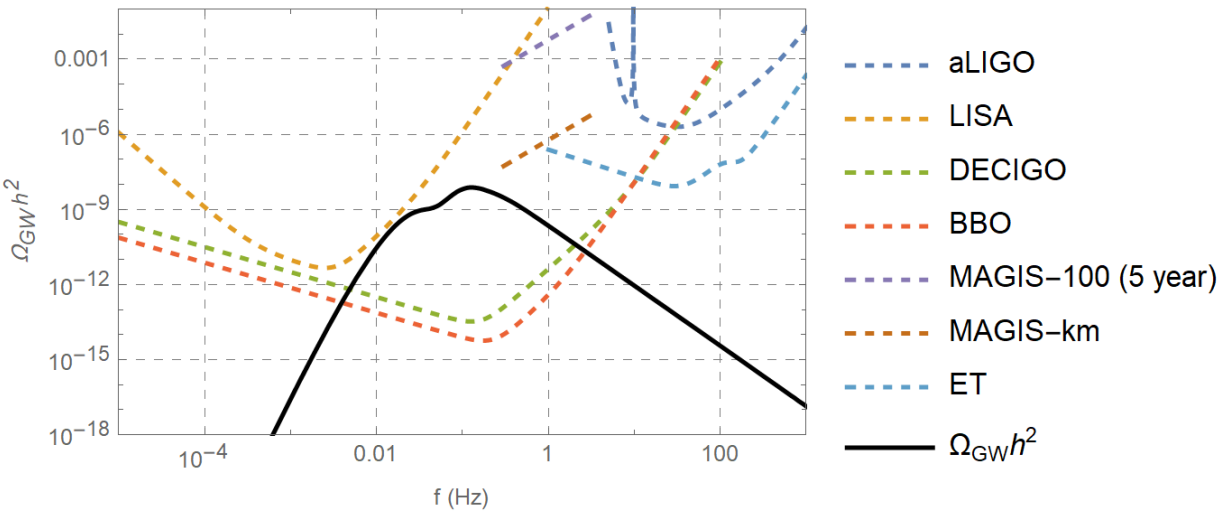

Figure 5.7: The black thick line represents the energy density parameter $\Omega_{GW}h^2$ as a function of the GW frequency computed from the Fibre Inflation primordial power spectrum. The dashed lines represent the sensitivity curves for aLIGO, LISA, DECIGO, BBO, MAGIS-100, MAGIS-km, and ET.

large scales $k \in [\sim 10^{13}, \sim 10^{17}]$, see figure (5.6). It is easy to establish a relation between the GW frequency, the mass of PBHs and the scale using Eqs. (5.5), (5.6) and the fact that $k \sim a \sim e^{\Delta N}$, obtaining, as one should expect, $k \sim f$. Then since we have the correspondence $\Omega_{GW} \sim \mathcal{P}_h \sim \mathcal{P}_u^2$ we obtain $\Omega_{GW} \sim f^{-2.4}$, which is what we computed. For the lower frequencies it was not possible to perform a similar fit since we see from figure (5.3) that the behaviour of the scalar power spectrum at scales corresponding to $N \approx 19 - 26$ efoldings before the end of inflation (or $k \sim 10^{10} - 10^{12}$) cannot be approximated with a function of the kind $\mathcal{P}_u(k) \sim k^{\alpha}$.

5.2.1 Comparison with current observational bounds

Comparing the plot in the right panel of figure (5.4) with figure (4.4) we see that our peak mass is around $\sim 10^{-15} M_{\odot}$, which is a value that does not have observational bounds for the mass of PBHs. As the mass increases we find the some constraints due to the existence of white dwarves for $M_{PBH} \sim 10^{-14} - 10^{-13} M_{\odot}$ which however do not influence our results since the contribution to the total DM abundance for PBHs of this mass is between 10% and 100% [44]. There are no constraints until $M_{PBH} \sim 10^{-11} - 10^{-10} M_{\odot}$. These values correspond to $\Omega_{GW}(\tau_0, M_{PBH})h^2 \sim 10^{-15} - 10^{-16}$, which are out of reach of current and future interferometers.

5.2.2 Comparison with interferometry sensitivity curves

In figure (5.7) we compare the energy density parameter $\Omega_{GW}h^2$ as a function of the GW peak frequency with the sensitivity curves of these interferometers. We see that it is just

out of reach of LISA, ET and MAGIS-km, but the future experiments DECIGO and BBO could detect these gravitational waves.

As we said before the scales higher than $k \sim 10^{16} - 10^{17}$ are not reliable, however they correspond to GW frequencies of order $f \sim 10^5 - 10^6$ Hz. This can be proved relating the GW frequency f_{GW} in Eq. (5.6) with the scales k using Eq. (5.5) and the fact that $a = \exp(\Delta N) = k/H$. The Hubble parameter H is always of order $\mathcal{O}(10^{-5} - 10^{-6})$ during inflation (as it can be seen from the left panel of figure (5.2)) and inserting the numerical values for the number of relativistic degrees of freedom at formation time and at present time one finds the result:

$$f_{GW} \sim (10^{-11} - 10^{-12}) \cdot k \text{ Hz}$$

We then conclude that our results are reliable within the frequency domains of current and future interferometers, so that they can be compared with observations.

Chapter 6

Conclusions

The objective of this thesis was the study of gravitational wave production in Fibre Inflation. These would have been generated after the gravitational collapse of the density perturbations to form primordial black holes during inflation.

The first chapter was devoted to a general introduction to the ideas and tools that were used in this thesis. We also defined our units and notations.

In the second chapter we studied standard cosmology. We started from the assumption of homogeneous and isotropic universe, namely the Cosmological Principle, which uniquely determines the spacetime metric to be of the FRW type. Exploiting the continuity equation for the stress-energy tensor and inserting the metric into the Einstein field equations we obtained the Friedmann equations for the evolution in time of the scale factor. We analyzed three typical cases, namely dust, radiation and vacuum energy, and we found that for a flat FRW spacetime the third case allows for an accelerated expansion of the universe. We then enlightened some of the problems that afflict this model, namely the flatness, the horizon and the exotic particles problem, and we showed how a period of accelerated expansion of the universe solves them simultaneously.

In the third chapter we studied inflation in detail, showing that a scalar field, the inflaton, can drive it if its potential is sufficiently smooth and flat. We studied the evolution of the background, which obeys a Klein-Gordon-like equation, and we saw how its coupling with the gravitational field induces inflation. After that we briefly studied the theory of cosmological perturbations, showing how it can be used to study small variations around the flat FRW metric. This led us to a form of the metric that contains both scalar and tensor modes, which are of interest for us in the study of gravitational wave production. We then moved to study the curvature perturbations and we derived the Mukhanov-Sasaki equation, which describes the evolution in (conformal) time of their Fourier modes. Their quantization is then performed and we saw how the non-uniqueness of the vacuum, a typical feature of the theory of quantum fields in a curved background, can be removed setting some initial conditions for the modes: we adopted the Bunch-Davies conditions. We then defined the scalar and the tensor power spectra and we reported their observational constraints. We devoted the final section of the chapter to the description of dark matter and the problem that its introduction as a component of the total energy density of the universe solves. We proposed that it is made of primordial black holes and we studied their production mechanism and gave some estimates on the primordial power spectrum in order

for this process to actually occur.

In the fourth chapter we introduced the theory of secondary gravitational waves using the metric derived in the previous chapter when we dealt with cosmological perturbation theory. We derived an expression for the energy density parameter for gravitational waves and we computed it for some examples of primordial power spectra. We then described the current observational bounds on the fraction of PBH DM and the interferometry sensitivity curves and we compared them with the results from the examples.

Finally in the fifth chapter we introduced Fibre Inflation, an inflationary model derived from string theory in the framework of type IIB flux compactification. In this model the scalar power spectrum is computed numerically solving the Mukhanov-Sasaki equation for the curvature perturbations and it presents a peak of order $\mathcal{O}(10^{-2})$ that allows for the formation of primordial black holes. We then inserted this power spectrum into the expression for the energy density parameter for gravitational waves and analyzed the results. We found that the peak is at a frequency of order $\mathcal{O}(10^{-1})$ Hz, which is in the frequency domain of current and future experiments such as LISA, DECIGO, BBO and ET. We then compared it with their sensitivity curves, finding that the stochastic background of gravitational waves derived in this framework is just out of reach of LISA. In order for the signal to be detected by this experiment the mass of primordial black holes produced in Fibre Inflation should be higher: this would allow for the peak to be around a lower frequency and hence detectable. However this would mean that the inflection point should be at field values that are further from the minimum than the one that we considered in this thesis and this has problems related to the spectral index. In Fibre Inflation this quantity turns out to be a bit too red (it can be fixed for example adding non-zero neutrino masses) and the change of the position of the inflection point we just mentioned would make it even redder. Also a higher PBH mass would be subjected to the observational constraints mentioned in chapter 4: we then conclude that to detect these gravitational waves we need to rely on other detectors.

Among these there are DECIGO and BBO: in fact their sensitivities allow for the detection of the signal we computed in chapter 5. This is an important result since it provides a connection between an observable quantity predicted from string theory and experiments: we could then be able to test the theory and check the validity of our result.

We studied dark matter as primordial black holes because this hypothesis does not rely on modified gravity theory nor physics in beyond the SM in their production mechanism. Also the primordial power spectrum is derived from a top down approach as a low energy effective 4D theory whose UV limit is string theory and not given as an ansatz as it is done in the three examples we studied in chapter 4 (δ function, top hat function and broken power law). These are two appealing features that enlighten the robustness of the model we considered. Finally we stress that the inflaton potential has a rich structure that allows for the production primordial black holes. Among the parameters that can be tuned there are some concerning the details of string compactification: this can be a way to explore the string landscape and thus to make a connection between string compactification and string phenomenology with observation.

Appendix A

Calculations for the broken power law potential

Here we present the details of the computation of the energy density parameter for GWs for the case of the broken power law potential Eq. (4.4).

The two terms in the integral are written as:

$$\mathcal{P}_\zeta^{\rm BPL}\left(\frac{\sqrt{3}}{2}k(s\pm d)\right)=\mathcal{A}^2\left(\frac{\sqrt{3}k}{2k_p}(s\pm d)\right)^{n_+}\theta\left(\frac{\sqrt{3}}{2}k(s\pm d)-k_p\right)+...$$

$$...+\mathcal{A}^2\left(\frac{\sqrt{3}k}{2k_p}(s\pm d)\right)^{n_-}\theta\left(k_p-\frac{\sqrt{3}}{2}k(s\pm d)\right),$$

so that the product of the two $\mathcal{P}_\zeta$ terms in the integral becomes:

$$\mathcal{P}_\zeta^{\rm BPL}\left(\frac{\sqrt{3}}{2}k(s+d)\right)\mathcal{P}_\zeta^{\rm BPL}\left(\frac{\sqrt{3}}{2}k(s-d)\right)=$$

$$\mathcal{A}^4\left(\frac{3k^2}{4k_p^2}\right)^{n_+}(s^2-d^2)^{n_+}\theta\left(\frac{\sqrt{3}}{2}k(s+d)-k_p\right)\theta\left(\frac{\sqrt{3}}{2}k(s-d)-k_p\right)+...$$

$$...+\mathcal{A}^4\left(\frac{\sqrt{3}k}{2k_p}\right)^{n_++n_-}(s+d)^{n_+}(s-d)^{n_-}\theta\left(\frac{\sqrt{3}}{2}k(s+d)-k_p\right)\theta\left(k_p-\frac{\sqrt{3}}{2}k(s-d)\right)+...$$

$$...+\mathcal{A}^4\left(\frac{\sqrt{3}k}{2k_p}\right)^{n_++n_-}(s+d)^{n_-}(s-d)^{n_+}\theta\left(k_p-\frac{\sqrt{3}}{2}k(s+d)\right)\theta\left(\frac{\sqrt{3}}{2}k(s-d)-k_p\right)+...$$

$$...+\mathcal{A}^4\left(\frac{3k^2}{4k_p^2}\right)^{n_-}(s^2-d^2)^{n_-}\theta\left(k_p-\frac{\sqrt{3}}{2}k(s+d)\right)\theta\left(k_p-\frac{\sqrt{3}}{2}k(s-d)\right). \qquad \text{(A.1)}$$

Once we have the expression in Eq. (A.1) for the product of the two power spectra in the integrand the θ functions give some conditions on the domains of integration. First of all we

impose the condition $k < 2k_p$ [20], then necessarily it must hold $Q > 1/\sqrt{3}$, where we have defined $Q := 2k_p/(\sqrt{3}k)$. The Heaviside θ functions, together with the integration domains $s \in [1/\sqrt{3}, \infty]$, $d \in [0, 1\sqrt{3}]$, give the following conditions to the domains of integration of the four terms in Eq. (A.1):

$$\text{First term:} \begin{cases} s+d \geq Q \\ s-d \geq Q \end{cases} \implies \begin{cases} [Q \leq s \leq Q+1/\sqrt{3} \ \wedge \ 0 \leq d \leq s-Q] \cup \\ [Q+1/\sqrt{3} \leq s < \infty \ \wedge \ 0 \leq d \leq 1/\sqrt{3}] \end{cases}$$

$$\text{Second term:} \begin{cases} s+d \geq Q \\ s-d \leq Q \end{cases} \implies \begin{cases} [1/\sqrt{3} \leq s \leq Q \ \wedge \ Q-s \leq d \leq 1/\sqrt{3}] \cup \\ [Q \leq s \leq Q+1/\sqrt{3} \ \wedge \ s-Q \leq d \leq 1/\sqrt{3}] \end{cases}$$

$$\text{Third term:} \begin{cases} s+d \leq Q \\ s-d \geq Q \end{cases} \implies \emptyset,$$

Fourth term:

$$\begin{cases} s+d \leq Q \\ s-d \leq Q \end{cases} \implies \begin{cases} [1/\sqrt{3} \leq s \leq \ Q \ \wedge \ 0 \leq d \leq Q-s] & \text{if } Q \leq 2/\sqrt{3} \\ \begin{cases} [1/\sqrt{3} \leq s \leq \ Q-1/\sqrt{3} \ \wedge \ 0 \leq d \leq Q-1\sqrt{3}] \cup \\ [Q-1/\sqrt{3} \leq s \leq Q \ \wedge \ 0 \leq d \leq s-Q] \end{cases} & \text{if } Q > 2/\sqrt{3} \end{cases}$$

The final result can then be written as the sum of three integrals:

$$\frac{36}{c_g \Omega_{r,0}} \Omega_{GW}(\tau_0, k) = I_1 + I_2 + I_3,$$

where:

$$\mathcal{A}^{-4} \left(\frac{3}{4}\frac{k^2}{k_p^2}\right)^{-n_+} I_1 = \left(\int_Q^{Q+1/\sqrt{3}} \mathrm{d}s \int_0^{s-Q} \mathrm{d}d + \int_{Q+1/\sqrt{3}}^{\infty} \mathrm{d}s \int_0^{1/\sqrt{3}} \mathrm{d}d\right) \ i_1(s,d),$$

$$\mathcal{A}^{-4} \left(\frac{\sqrt{3}}{2}\frac{k}{k_p}\right)^{-(n_+ + n_-)} I_2 = \left(\int_{1/\sqrt{3}}^{Q} \mathrm{d}s \int_{Q-s}^{1/\sqrt{3}} \mathrm{d}d + \int_Q^{Q+1/\sqrt{3}} \mathrm{d}s \int_{s-Q}^{1/\sqrt{3}} \mathrm{d}d\right) \ i_2(s,d),$$

$$\mathcal{A}^{-4} \left(\frac{3}{4}\frac{k^2}{k_p^2}\right)^{-n_-} I_3 = \theta\left(\frac{2}{\sqrt{3}} - Q\right) \int_{1/\sqrt{3}}^{Q} \mathrm{d}s \int_0^{Q-s} \mathrm{d}d \ i_3(s,d) + ...$$

$$... + \theta\left(Q - \frac{2}{\sqrt{3}}\right) \left(\int_{1/\sqrt{3}}^{Q-1/\sqrt{3}} \mathrm{d}s \int_0^{Q-1/\sqrt{3}} \mathrm{d}d + \int_{Q-1/\sqrt{3}}^{Q} \mathrm{d}s \int_0^{s-Q} \mathrm{d}d\right) \ i_3(s,d),$$

and:

$$i_1(s,d) = \left(d^2 - \frac{1}{3}\right)^2 \left(s^2 - \frac{1}{3}\right)^2 (s^2-d^2)^{n_+-2} \left[\mathcal{I}_c^2(s,d) + \mathcal{I}_s^2(s,d)\right]$$

$$i_2(s,d) = \left(d^2 - \frac{1}{3}\right)^2 \left(s^2 - \frac{1}{3}\right)^2 (s+d)^{n_+-2}(s-d)^{n_--2} \left[\mathcal{I}_c^2(s,d) + \mathcal{I}_s^2(s,d)\right]$$

$$i_3(s,d) = \left(d^2 - \frac{1}{3}\right)^2 \left(s^2 - \frac{1}{3}\right)^2 (s^2-d^2)^{n_--2} \left[\mathcal{I}_c^2(s,d) + \mathcal{I}_s^2(s,d)\right]$$

Also note that:

$$\theta\left(\pm\left(Q-\frac{2}{\sqrt{3}}\right)\right)=1\Longleftrightarrow\pm k>\pm k_p.$$

Let us begin expanding $i_1(s,d)$:

$$i_1=\pi^2\theta(s-1)(s^2-d^2)^{n_+-8}\sum_{m=0}^{6}\left(d^{2m}f_m(s)\right)+\left(\log\frac{1-d^2}{|s^2-1|}\right)^2(s^2-d^2)^{n_+-8}\sum_{m=0}^{6}\left(d^{2m}f_m(s)\right)+...$$

$$...+4(s^2-d^2)^{n_+-6}\sum_{m=0}^{4}\left(d^{2m}g_m(s)\right)+4\log\frac{1-d^2}{|s^2-1|}(s^2-d^2)^{n_+-7}\sum_{m=0}^{5}\left(d^{2m}h_m(s)\right), \quad \text{(A.2)}$$

where f_m, g_m and h_m are the following even polynomials:

$$f_0(s)=\frac{16}{81}-\frac{128}{81}s^2+\frac{40}{9}s^4-\frac{440}{81}s^6+\frac{265}{81}s^8-\frac{26}{27}s^{10}+\frac{1}{9}s^{12},$$

$$f_1(s)=-\frac{128}{81}+\frac{112}{9}s^2-\frac{920}{27}s^4+\frac{3220}{81}s^6-\frac{610}{27}s^8+\frac{56}{9}s^{10}-\frac{2}{3}s^{12},$$

$$f_2(s)=\frac{40}{9}-\frac{920}{27}s^2+\frac{2402}{27}s^4-\frac{2564}{27}s^6+\frac{431}{9}s^8-\frac{34}{3}s^{10}+s^{12},$$

$$f_3(s)=-\frac{440}{81}+\frac{3220}{81}s^2-\frac{2564}{27}s^4+\frac{752}{9}s^6-\frac{92}{3}s^8+4s^{10},$$

$$f_4(s)=\frac{265}{81}-\frac{610}{27}s^2+\frac{431}{9}s^4-\frac{92}{3}s^6+6s^8,$$

$$f_5(s)=-\frac{26}{27}+\frac{56}{9}s^2-\frac{34}{3}s^4+4s^6,$$

$$f_6(s)=\frac{1}{9}-\frac{2}{3}s^2+s^4;$$

$$g_0(s)=\frac{4}{81}-\frac{28}{81}s^2+\frac{61}{81}s^4-\frac{14}{27}s^6+\frac{1}{9}s^8,$$

$$g_1(s)=-\frac{28}{81}+\frac{194}{81}s^2-\frac{46}{9}s^4+\frac{10}{3}s^6-\frac{2}{3}s^8,$$

$$g_2(s)=\frac{61}{81}-\frac{46}{9}s^2+\frac{94}{9}s^4-6s^6+s^8,$$

$$g_3(s)=-\frac{14}{27}+\frac{10}{3}s^2-6s^4+2s^6,$$

$$g_4(s)=\frac{1}{9}-\frac{2}{3}s^2+s^4;$$

$$h_0(s) = -\frac{8}{81} + \frac{20}{27}s^2 - \frac{50}{27}s^4 + \frac{145}{81}s^6 - \frac{20}{27}s^8 + \frac{1}{9}s^{10},$$

$$h_1(s) = \frac{20}{27} - \frac{148}{27}s^2 + \frac{361}{27}s^4 - \frac{332}{27}s^6 + \frac{43}{9}s^8 - \frac{2}{3}s^{10},$$

$$h_2(s) = -\frac{50}{27} + \frac{361}{27}s^2 - \frac{280}{9}s^4 + \frac{232}{9}s^6 - \frac{26}{3}s^8 + s^{10},$$

$$h_3(s) = \frac{145}{81} - \frac{332}{27}s^2 + \frac{232}{9}s^4 - 16s^6 + 3s^8,$$

$$h_4(s) = -\frac{20}{27} + \frac{43}{9}s^2 - \frac{26}{3}s^4 + 3s^6,$$

$$h_5(s) = \frac{1}{9} - \frac{2}{3}s^2 + s^4.$$

The integrations of the first and the third terms over the variable d are given by this general expression:

$$\int_\alpha^\beta \mathrm{d}d\, d^a (s^2 - d^2)^{n_+ - b} = \frac{d^{a+1} s^{-a} (s^a - d^2)^{n_+ - b + 1}}{a+1} {}_2F_1\left(1, \frac{a - 2b + 3}{2} + n_+; \frac{a+3}{2}; d^2 s^{-a}\right)\Bigg|_{d=\alpha}^{d=\beta},$$

where ${}_2F_1$ is the hypergeometric function. For the other two terms we could not find any analytic expression due to the presence of the logarithm.

The computation of I_3 is analogous, with n_- instead of n_+.

For I_2 we have the same terms as in Eq. (A.2), but with $(s^2 - d^2)^{n_+}$ exchanged with $(s+d)^{n_+}(s-d)^{n_-}$. The integrations over the variable d give the following general expression for the first and third terms:

$$\int_\alpha^\beta \mathrm{d}d\; d^a (s+d)^{n_+ - b} (s-d)^{n_- - b} =$$

$$\frac{d^{a+1}}{a+1}\left(1 - \frac{d^2}{s^2}\right)^b \left(1 - \frac{d}{s}\right)^{-n_-} (s-d)^{n_- - b} (s+d)^{n_+ - b} \left(\frac{d+s}{s}\right)^{-n_-} \cdot \ldots$$

$$\ldots \cdot F_1\left(a+1, b - n_+, b - n_-; a+2; \frac{d}{s}, -\frac{d}{s}\right)\Bigg|_{d=\alpha}^{d=\beta},$$

where F_1 is the first Appell hypergeometric series. Again for the other two terms we could not find an analytical expression due to the presence of the logarithm.

The integration over s must then be carried over numerically since we were not able to find an analytical expression due to their very complicated form.

Acknowledgements

I would like to thank everyone that in any way and for any reason helped and supported me during these years. I am particularly grateful to my supervisor Michele Cicoli and my co-supervisor Francisco G. Pedro: they showed a lot of passion in this work and helped me through in this endeavour with kindness and devotion. I would like to thank all my professors who give their time to teach us students this subject that never stops fascinating us.

Last but not least I want to thank my family and my friends for their incredible support. A special thank goes to N. for being wonderful.

Bibliography

[1] D. Mukhanov. *Physical Foundations of Cosmology*. Cambridge University Press, 2019.

[2] D. Tong. *Lecture notes on Cosmology*. 2019.

[3] R. d'Inverno. *Introducing Einstein Relativity*. Clarendon Press, Oxford, 1992.

[4] S. Weinberg. *Gravitation and Cosmology: Principles and Applications of the General Theory of Relativity*. John Wiley and Sons, 1972.

[5] P. R. Ade *et al.* [Planck Collaboration]. *Planck 2015 results. XIII. Cosmological Parameters*. arXiv:1502.01589v3, 2014.

[6] D. V. Schroeder M. E. Peskin. *An Introduction to Quantum Field Theory*. Reading, Massachussetts: Perseus Books, 1995.

[7] M. Srednicki. *Quantum Field Theory*. Cambridge University Press, 2007.

[8] P.C.W. Davies N. D. Birrell. *Quantum Fields in Curved Space*. Cambridge University Press, 1982.

[9] S. Winitzki V. Mukhanov. *Introduction to Quantum Effects in Gravity*. Cambridge University Press, 2007.

[10] A. Riotto D. H. Lyth. *Particle Physics Models of Inflation and the Cosmological Density Perturbations*. arXiv:hep-ph/9807278v4, 1999.

[11] A. Riotto. *Inflation and the Theory of Cosmological Perturbations*. arXiv:hep-ph/0210162v2, 2017.

[12] S. M. Carroll *et al. The Cosmology of Generalized Modified Gravity Models*. arXiv:astro-ph/0410031v2, 2005.

[13] A. de Felice. *f(R) theories*. arXiv:1002.4928v2, 2010.

[14] M. Maggiore. *Gravitational Waves, volume 2: Astrophysics and Cosmology*. Oxford University Press, 2018.

[15] S. Yoshiura *et al. Constraints on Primordial Power Spectrum from Galaxy Luminosity Functions*. arXiv:2007.14695v2, 2020.

[16] C. Unal J. García-Bellido M. Peloso. *Gravitational Wave signatures of inflationary models from Primordial Black Hole Dark Matter*. arXiv:1707.02441v1, 2017.

[17] N. Aghanim *et al. Planck 2018 results. VI. Cosmological Parameters*. arXiv:1807.06209v3, 2018.

[18] K. Freese. *Review of Observational Evidence for Dark Matter in the Universe and in Upcoming Searches for Dark Stars*. arXiv:0812.4005v1, 2008.

[19] S. Hawking. "Gravitationally Collapsed Objects of Very Low Mass". In: *Mon. Not. R. astr. Soc.* 152 (1971), pp. 75–78.

[20] J. Yokoyama R. Saito. *Gravitational-Wave Constraints on the Abundance of Primordial Black Holes*. arXiv:0912.5317v2, 2011.

[21] S. Hawking. "Black hole explosions?" In: *Nature* 248 (1974), p. 30.

[22] F. G. Pedro M. Cicoli V. A. Diaz. *Primordial Black Holes from String Inflation*. arXiv:1803.02837v2, 2018.

[23] A. Riotto J. R. Espinosa D. Racco. *A Cosmological Signature of the Higgs Instability: Gravitational Waves*. arXiv:1804.07732v3, 2019.

[24] K. Takahashi D. Baumann P. Steinhardt. *Gravitational Waves Spectrum Induced by Primordial Scalar Perturbations*. arXiv:hep-th/0703290v1, 2007.

[25] D. Wands K. N. Ananda C. Clarkson. *The cosmological gravitational wave background from primordial density perturbations*. arXiv:gr-qc/0612013v1.

[26] N. Bartolo *et al. The Primordial Black Hole Dark Matter: LISA Serendipity*. arXiv: 1810.12218v3, 2018.

[27] B.J. Carr *et al. New Cosmological Constraints on Primordial Black Holes*. arXiv:0912. 5297v2, 2010.

[28] J. Varela P. W. Graham S. Rajendran. *Dark Matter Triggers on Supernovae*. arXiv: 1505.04444v1, 2015.

[29] H. Niikura *et al. Microlensing constraints on primordial black holes with the Subaru/HSC Andromeda observation*. arXiv:1701.02151v3, 2018.

[30] M. J. Lehner K. Griest A. M. Cieplak. "New Limits on Primordial Black Hole Dark Matter from an Analysis of Kepler Source Microlensing Data". In: *Phys. Rev. Lett.* 111, 181302 (2013).

[31] P. Tisserand *et al. Limits on the Macho Content of the Galactic Halo from the EROS-2 Survey of the Magellanic Clouds*. arXiv:astro-ph/0607207v2, 2007.

[32] T. D. Brandt. *Constraints on MACHO Dark Matter from Compact Stellar Systems in Ultra Faint Dwarf Galaxies*. arXiv:1605.03665v2, 2016.

[33] M. Kamionkowski T. Ali-Haïmoud. *Cosmic microwave background limits on accreting primordial black holes*. arXiv:1612.06544v2, 2017.

[34] R. Flauger D. Aloni K. Blum. *Cosmic microwave background constraints on primordial black hole dark matter*. arXiv:1612.03811v2, 2017.

[35] B. Horowitz. *Revisiting Primordial Black Holes Constraints from Ionization History*. arXiv:1612.07264v1, 2016.

[36] C. P. L. Berry C. J. Moore R. H. Cole. *Gravitational-wave Sensitivity Curves*. arXiv:1408.0740v2, 2014.

[37] A. G. Riess J. Soltis S. Casertano. *The Parallax of ω Centauri Measured from Gaia EDR3 and a Direct, Geometric Calibration of the Tip of the Red Giant Branch and the Hubble Constant*. arXiv:2012.09196v1, 2020.

[38] C. Liu T. Robson N. J. Cornish. *The construction and use of LISA sensitivity curves*. arXiv:1803.01944v2, 2018.

[39] N. Seto K. Yagi. *Detector configuration of DECIGO/BBO and identification of cosmological neutron-star binaries*. arXiv:1101.3940v2, 2017.

[40] J. Coleman. *Matter-wave Atomic Gradiometer Interferometric Sensor (MAGIS-100) at Fermilab*. arXiv:1812.00482v1, 2018.

[41] P. Adamson *et al. PROPOSAL: P-1101, Matter-wave Atomic Gradiometer Interferometric Sensor (MAGIS-100)*. Fermilab-tm-2700-ppd, 2018.

[42] B. F. Schutz B. S. Sathyaprakash. *Physics, Astrophysics and Cosmology with Gravitational Waves*. arXiv:0903.0338v1, 2009.

[43] F. Quevedo M. Cicoli C. P. Burgess. *Fibre Inflation: Observable Gravity Waves from IIB Compactification*. arXiv:0808.0691v3, 2012.

[44] M. Sasaki *et al. Primordial Black Holes - Perspectives in Gravitational Wave Astronomy* -. arXiv:1801.05235v1, 2018.